Can we use atmospheric CO_2 measurements to verify emission trends reported by cities? Lessons from a six-year atmospheric inversion over Paris

Jinghui Lian[1,2], Thomas Lauvaux[3], Hervé Utard[1], François-Marie Bréon[2], Grégoire Broquet[2], Michel Ramonet[2], Olivier Laurent[2], Ivonne Albarus[1,2], Mali Chariot[2], Simone Kotthaus[4], Martial Haeffelin[4], Olivier Sanchez[5], Olivier Perrussel[5], Hugo Anne Denier van der Gon[6], Stijn Nicolaas Camiel Dellaert[6], and Philippe Ciais[2,7]

[1] Origins.earth, SUEZ Group, Tour CB21, 16 Place de l'Iris, 92040 Paris La Défense Cedex, France
[2] Laboratoire des Sciences du Climat et de l'Environnement (LSCE), IPSL, CEA-CNRS-UVSQ, Université Paris-Saclay, 91191 Gif sur Yvette Cedex, France
[3] Groupe de Spectrométrie Moléculaire et Atmosphérique (GSMA), Université de Reims-Champagne Ardenne, UMR CNRS 7331, Reims, France
[4] Institut Pierre Simon Laplace (IPSL), CNRS, École Polytechnique, Institut Polytechnique de Paris, 91128 Palaiseau Cedex, France
[5] AirParif, 7 rue Crillon, Paris, France
[6] Department of Climate, Air and Sustainability, TNO, P.O. Box 80015, 3508 TA Utrecht, Netherlands
[7] Climate and Atmosphere Research Center (CARE-C), The Cyprus Institute, 20 Konstantinou Kavafi Street, 2121, Nicosia, Cyprus

Correspondence to: Jinghui Lian (jinghui.lian@suez.com)

Abstract. Existing CO_2 emissions reported by city inventories usually lag real-time by a year or more and are prone to large uncertainties. This study responds to the growing need for timely and precise estimation of urban CO_2 emissions to support the present and future mitigation measures and policies. We focus on the Paris metropolitan area, the largest urban region in the European Union and the city with the densest atmospheric CO_2 observation network in Europe. We performed long-term atmospheric inversions to quantify the citywide CO_2 emissions, both fossil fuel and biogenic sources and sinks, over six years (2016-2021) using a Bayesian inverse modeling system. Our inversion framework benefits from a novel near-real-time hourly fossil fuel CO_2 emission inventory (Origins.earth) at 1 km spatial resolution. In addition to the mid-afternoon observations, we attempt to assimilate morning CO_2 concentrations based on the ability of the WRF-Chem transport model to simulate atmospheric boundary layer dynamics constrained by observed layer heights. Our results show a long-term decreasing trend by around 2%±0.6% per year in annual CO_2 emissions over the Paris region. The impact of COVID-19 pandemic led to a 13%±1% reduction in annual fossil fuel CO_2 emissions in 2020 with respect to 2019. Then, annual emissions increased by 5.2%±14.2% from 32.6±2.2 $MtCO_2$ in 2020 to 34.3±2.3 $MtCO_2$ in 2021. Based on a combination of up-to-date inventories, high-resolution atmospheric modeling, and high-precision observations, our current capacity could deliver near real-time CO_2 emission estimates at city scale in less than a month, and the results agree within 10% with independent estimates from multiple city-scale inventories.

1 Introduction

Most countries have actively committed to the 2015 Paris Agreement to limit global warming to well below 2°C, preferably 1.5°C, compared to pre-industrial levels. To achieve this goal, governments have pledged to implement stringent climate actions to reduce their national emissions with the ultimate objective of reaching climate neutrality by 2050. Cities account for more than 70% of annual global fossil fuel CO_2 emissions and thus are key areas for mitigating CO_2 emissions (Seto et al., 2014). To date, many

metropolitan areas have pledged and began to implement policies to achieve net-zero emissions (e.g., C40 city, GCoM). The choice of mitigation actions, for cost-effectiveness and to maximize emission reduction impact, depends mainly on the qualitative and quantitative understanding of urban emission sources with temporal-spatial details to understand evolving emission trends (Lauvaux et al., 2020; Mueller et al., 2021). However, the bottom-up carbon emissions based on public protocols for cities are prone to large uncertainties (Gurney et al., 2021). High-resolution gridded CO_2 emission inventories, e.g., the Hestia dataset for some US cities (Gurney et al., 2019) or the LAEI dataset for Greater London (Greater London Authority, 2021), could provide a detailed description of emissions from urban domains. This approach relies on a collection of extensive activity data and emission factors, and thus can be labor-intensive and time-consuming, especially for doing regular updates. Recently, Carbon Monitor Cities has been developed to provide near-real-time city-level CO_2 emissions for 1500 global cities from 2019 to 2021 (Huo et al., 2022). The quantification of greenhouse gas (GHG) emissions from atmospheric measurements offers accounting complementary to the conventional bottom-up approach (Ciais, 2010). These methods combine atmospheric measurements with bottom-up inventories through ~~atmospheric~~ inversion techniques (Tarantola, 2005). The scientific capabilities evolve rapidly with ~~the deployment of dense networks and~~ increasing model performances (~~Davis et al., 2017;~~ Deng et al., ~~2017;~~ 2017) and the deployment of dense networks in cities, e.g., Washington DC-Baltimore Metropolitan Areas (Karion et al., 2020), San Francisco Bay Area (Turner et al., ~~2020~~2020), Los Angeles (Yadav et al., 2021), Indianapolis (Davis et al., 2017), Paris, Munich and Zurich (https://www.icos-cp.eu/projects/icos-cities). The robustness of the inversion and the derived emission estimates need to be evaluated over periods of several months and years to check the stability and relevance of the seasonal cycle and of the inter-annual variability. For example, Mc Kain et al. (2012) indicated that their transport model showed a poor performance in modeling urban sites, so that only relative changes in the emission estimates were considered relevant. To our knowledge, ~~only three relatively long time series of~~few estimates of city GHG emissions have been published when based on long-term tower-based measurements and atmospheric inversion systems ~~have been published,~~. These include studies covering a period over one to ~~three~~five years for the cities of Paris, Boston ~~and,~~ Indianapolis and Los Angeles (Staufer et al., 2016; Sargent et al., 2018; Lauvaux et al. 2020; Yadav et al., 2023).

The Paris region, known as "Île-de-France" (IdF), is the highest populated and most economically active French region. Covering only 2% of the French territory, it has around 18% of the French population (12.2 over 67.8 million inhabitants), and produces 31% of the national GDP and 10% of the human-caused GHG emissions of France (source: AirParif https://www.airparif.asso.fr/en/monitor-pollution/emissions; CITEPA https://www.citepa.org/fr/2022-co2e/). Paris is one of the most active cities in tackling climate change and part of the C40 City consortium. The first Paris Climate Plan was adopted in 2007 and targeted a 25% reduction in GHG emissions by 2020 with respect to 2004 levels. Paris city also has an ambitious 2020-2030 action plan which targets a 50% decrease in local direct GHG emissions (Scope 1) compared to 2004 levels (Le Plan Climat de Paris, 2020). According to the AirParif (official air quality agency of the Paris region, https://www.airparif.asso.fr/en/) inventory, the contribution of each of the main GHG (in term of CO_2 equivalent emission) is 94% for CO_2, 4% for N_2O and 2% for CH_4 in 2010 (AirParif, 2013). Regarding atmospheric CO_2 monitoring capability, Paris is an important pilot city with the densest and most comprehensive atmospheric CO_2 measurements in Europe (e.g., Lopez et al., 2013; Xueref-Remy et al., 2018; Vogel et al., 2019; Lian et al., 2019). The Parisian ground-based network, whose first measurements date back to 2010, has grown from the initial three to the current seven high-precision continuous in-situ CO_2 monitoring stations. Over the past years, a series of studies have attempted to analyze the spatial-temporal variations of CO_2 concentrations over the Paris region and to monitor fossil fuel CO_2 emissions through an atmospheric inversion technique (Bréon et al., 2015; Wu et al., 2016; Staufer et al., 2016). Lian et al. (2022) estimated CO_2 emission reductions during COVID-19 confinements in Paris, which demonstrated the capability of the urban atmospheric monitoring system to identify significant emission changes (>20%) at short-term monthly timescales.

This study performs the first long-term atmospheric CO_2 inversions over the Paris metropolitan area and compares it to multiple city-scale inventories. It aims at assessing the ability and robustness of the inversion to track absolute urban CO_2 emission levels and its relative change over multiple years. The six years (2016-2021) continuous CO_2 measurements in Paris now provide sufficient information to investigate the variations in CO_2 emissions at different time scales (daily, seasonal and interannual) across an urban area. In addition to the mid-afternoon CO_2 concentration measurements that are commonly used for inversions, we also explore the potential for assimilating morning CO_2 data, taking into account the performance of the Weather Research and Forecasting Model coupled with a chemistry transport model (WRF-Chem, Grell et al., 2005) in capturing the evolution of the atmospheric boundary layer (ABL) dynamics. The height of the ABL is the main driver for uncertainties when assessing emissions from concentrations. This paper is organized as follows: Section 2 provides details of the city-scale Bayesian inversion methodology. Section 3 shows the variations in CO_2 emissions at different time scales. Section 4 summarizes the main conclusions and perspectives for further research.

2 Methods

A city-scale Bayesian inversion was conducted to quantify CO_2 emissions over a 6-year period spanning January 2016 to December 2021. The inversion system is based on atmospheric CO_2 measurements at seven in-situ stations combined with meteorological measurements, the WRF-Chem transport model run at 1 km × 1 km horizontal resolution (Lian et al., 2021), a near real-time fossil fuel CO_2 inventory produced by Origins.earth and the biogenic CO_2 fluxes simulated by the Vegetation Photosynthesis and Respiration Model (VPRM) included in WRF-Chem (Mahadevan et al., 2008). ~~The main principle of the Bayesian atmospheric inversion presented in Lian et al. (2022) is to optimize the 6-hour mean fossil fuel CO_2 emission budgets of the Greater Paris region (Figure 1) over four time windows per day (0:00-5:00, 6:00-11:00, 12:00-17:00, 18:00-23:00 UTC). The approach assimilates atmospheric CO_2 concentration differences between pairs of stations located upwind and downwind of the city to decrease the uncertainties caused by the transport of remote and natural fluxes outside the urban area.~~ Details regarding the inversion system setup are described in Lian et al. (2022) and outlined briefly below.

2.1 CO_2 measurement network

The seven stations are equipped with high-precision cavity ring-down spectroscopy (CRDS) CO_2 analyzers, together with an automated data processing and quality control system. CO_2 observations are calibrated every 1 to 6 months with standards traceable to the WMO CO_2 X2019 calibration scales (Hall et al., 2021). The precision of the one-hour average CO_2 concentration is better than 0.1 ppm (Xueref-Remy et al., 2018). These stations are distributed roughly along a northeast-southwest axis of the Paris urban area which coincides with the predominant wind directions (Figure 1).

~~Figures~~Figure 2 and Figure S1 ~~and S2~~ show the ~~daily and~~ monthly and daily average daytime (8-17 UTC) CO_2 concentrations at each in situ station from 2016 to 2021, respectively and in addition Figure ~~S2~~2 also shows the simulated background CO_2 concentration at SAC station using the CAMS CO_2 data set as boundary and initial inputs for WRF-Chem. The atmospheric background CO_2 concentrations have been steadily rising over the past 6 years, primarily attributed to global human activities. Generally, the average CO_2 concentrations across the network vary seasonally between 390 and 450 ppm. They are mainly driven by the atmospheric transport, the CO_2 biospheric cycle, and the proximity to the urban anthropogenic CO_2 emission sources. The interannual CO_2 variations depend primarily on the year-to-year variations in synoptic weather conditions, air temperature and the associated emissions. For example, the notably high CO_2 concentrations observed near the surface during the 2016/17 winter were

caused by stagnant, often stable atmospheric stratification associated with cold and dry air masses and low ventilation weather conditions over the north of France (Bulletin Climatique Météo-France, 2016 and 2017).

The gradients of CO_2 concentrations between the downwind and upwind stations are linked to the emissions within the Paris urban area. The CO_2 concentrations are significantly higher at the two urban stations CDS and JUS than those at peri-urban sites across all seasons (Figure ~~S2~~2). The magnitude in CO_2 gradients between urban and suburban areas is around 5~10 ppm in summer, increasing to 20~30 ppm during the winter months as a result of more stable atmospheric conditions (lower vertical dispersion and shallow ABLH) combined with high emissions from residential heating. The citywide CO_2 gradients across the Paris agglomerations have shown their potential in previous inversion studies to estimate the city-scale CO_2 emissions (Bréon et al., 2015; Staufer et al., 2016).

2.2 Origins.earth ~~inventory~~and other CO_2 inventories

Fossil fuel CO_2 a priori fluxes used in this study are taken from a patent pending high-resolution inventory produced by Origins.earth (https://www.origins.earth/) over the IdF region, in combination with the global Open-source Data Inventory for Anthropogenic CO_2 (ODIAC) product (Oda et al., ~~2019~~2018) in surrounding areas. The Origins.earth bottom-up inventory is a gridded map of fossil fuel CO_2 emissions within a rectangular (on a latitude and longitude grid) domain which encompasses most of the IdF region (Figure 1) at 1 km × 1 km spatial and hourly temporal resolution. It provides the Scope 1 CO_2 emissions from the year 2018 until the present time. For the simulation period from 2016 to 2017, we used CO_2 emissions from the Origins.earth inventory for the year 2018 as the WRF-Chem model inputs. The Origins.earth inventory includes more than 60 source types for carbon emission activities. These types of activities are grouped into six activity sectors (transportation, residential, tertiary, industry including cement, energy, and waste). The inventory compilation method is outlined in SI Appendix (Text S1).

The IdF is a large urban region with estimated annual fossil fuel CO_2 emissions exceeding 30 $MtCO_2$ per year, dominated by traffic and residential sectors. The spatial distributions of the emissions are shown in Figure 1. According to the Origins.earth inventory, the annual emission budgets of the residential sector are 11.0, 10.9, 10.1 and 11.4 $MtCO_2$, representing 32%, 34%, 35% and 38% of total emissions for 2018, 2019, 2020 and 2021 respectively. For the traffic sector averages are 12.3 $MtCO_2$ (36%), 10.9 $MtCO_2$ (33%), 8.7 $MtCO_2$ (30%) and 8.7 $MtCO_2$ (29%) from 2018 to 2021 (Figure ~~S3b~~S2b). Figure ~~S3a~~S2a shows the daily fossil fuel CO_2 emissions by sector and their respective proportions from 2018 to 2021. Generally, the temporal variations of CO_2 emissions from the building sector show a large seasonal cycle, mainly related to the heating demand that is linearly driven by the variations of air temperature below a threshold of ≈ 19°C. Emissions from the tertiary, industry and energy have a relatively flat seasonal variation.

In this study, the inverse emissions are compared to independent estimates from different inventories and a published study. These include (i) TNO-GHGco inventory at a resolution of 1/10º×1/20º (lon×lat) (~6 km×6 km) for the years 2005-2020 (Denier van der Gon et al., 2021), (ii) TNO-GHGco inventory at a resolution of 1/60º×1/120º (lon×lat) (~1 km×1 km) for the years 2015, 2017 and 2018 (Dellaert et al., 2019), (iii) AirParif inventory developed by the local official air quality agency ~~(https://www.airparif.asso.fr/en/)~~ at a 1 km × 1 km resolution for the years 2005, 2010, 2015 and 2018, (iv) the city-level CO_2 emissions from the Carbon Monitor Cities dataset (https://cities.carbonmonitor.org/, Huo et al., 2022) for the years 2019-2021, (v) Staufer et al. (2016) reported a full year (August 2010-July 2011) estimate of the IdF region fossil fuel CO_2 emissions by assimilating citywide CO_2 measurements from a sparse network of three stations with the inversion methodology. Here, we consider that these multiple emission estimates allow for a cross-validation as they were developed by several research groups using distinct data sources, methods and protocols.

2.3 Adding morning CO_2 data and ABL height selection

The accuracy of atmospheric inversion results depends to a large extent on the quality of the atmospheric transport model. The major uncertainties in CO_2 modeling are related to model errors in horizontal wind and vertical mixing within the atmospheric boundary layer (Kretschmer et al., 2012). A stringent data selection of CO_2 concentrations to be assimilated for the inversion is generally applied (e.g., Staufer et al., 2016; Wu et al., 2016; Lauvaux et al., 2020). The aim of the data selection is to rule out observations that are difficult to simulate accurately with the transport model. Previous studies (Staufer et al., 2016; Lian et al., 2022) assimilated only afternoon CO_2 data from 12 to 17 UTC during which the atmospheric boundary layer is expected to be well developed ~~with a constant height.~~ Moreover, the wind speeds at downwind stations are ~~imposed~~required to be higher than 3 m/s to minimize possible contaminations from local sources of CO_2 emissions near the measurement sites that cannot be reproduced by the model.

However, the selection of a limited number of suitable data produces more uncertain estimates over periods when no observations are selected. The high sensitivity of the inverse emissions to the diurnal variations of prior emissions also highlights the limitations induced by assimilating data only during the afternoon. Therefore, we attempt to include morning CO_2 concentration data in this study. Given that atmospheric models have difficulties in correctly reproducing the mixing processes under stable conditions and when the boundary layer develops in the morning, caution is required when assimilating morning CO_2 concentrations. We assumed that the ABL height could provide a good diagnostic to assess the vertical mixing and dilution associated with turbulence near the surface. We thus first evaluated the WRF-Chem simulated ABL heights against observations at the SIRTA station (Haeffelin et al., 2005) located about 20 km southwest of the Paris center (Figure 1). The modeled ABL heights were diagnosed from the potential temperature using the 1.5-theta-increase method (Nielsen-Gammon et al., 2008), while the aerosol-based STRATfinder algorithm (Kotthaus et al., 2020) was applied to derive ABL heights from attenuated backscatter profiles measured with an automatic lidar ceilometer (Lufft CHM15k).

Figure ~~S4~~S3 shows hourly ABL heights derived from both measurements and simulations from 2016 to 2021 for morning (8-11 UTC) and afternoon (12-17 UTC) periods, respectively. In general, the model captures reasonably well the ABL heights throughout the year with a fair correlation coefficient (>0.6). However, the simulated ABL heights are, on average, higher than the measurements with biases of 80~130m. This could reflect an overestimation of the atmospheric instability in the lowest atmospheric layer by WRF or may in fact indicate that vertical dilution of atmospheric tracers (here observed aerosol profiles) may lag behind the thermodynamic evolution of the ABL morning development (Text S2). Particularly large relative discrepancies are detected during the winter and morning periods associated with stable atmospheric conditions. This model-observation comparison of ABL heights allows us to revise the recent selection of CO_2 concentration measurements that can be assimilated into the inversion system as used in Lian et al. (2022) and extend it to the morning period~~.~~ (Figure S4). The revision consists primarily of adding two additional selection criteria concerning the morning data between 8-11 UTC. First, we discard the data when the relative error of the modeled ABL heights against observations is larger than 80%. This threshold was set based on the distributions of the relative errors in ABL shown in Figure ~~S4~~S3. Second, we apply a tighter filtering for the morning data (8-11 UTC) by increasing the minimum wind speed threshold to 5 m/s compared to the 3m/s used for the afternoon.

~~**In addition to the reference inversion (Text S3),**~~**2.4 Inversion configuration**

The main principle of the Bayesian atmospheric inversion presented in Lian et al. (2022) is to optimize the 6-hour mean fossil fuel CO_2 emission budgets of the Greater Paris region (within blue line in Figure 1) and the rest of the IdF region over four time windows per day (0:00-5:00, 6:00-11:00, 12:00-17:00, 18:00-23:00 UTC). The approach assimilates atmospheric CO_2

concentration gradients between pairs of stations located upwind and downwind of the city to decrease the uncertainties caused by the transport of remote and natural fluxes outside the urban area. The configurations of the atmospheric inversion system in this study are described in detail in Lian et al. (2022). It comprises the setup of the control vectors, the selection of the assimilated downwind-upwind CO_2 observation gradients (Figure S4), the assignments of the observation error and the prior flux uncertainties. Compared to Lian et al. (2022), only two minor modifications were made in this study in order to assess the impacts of morning CO_2 concentrations on the retrieved emissions: 1) Regarding the fossil fuel emissions, we assume a 60% relative uncertainty in the prior estimates of individual 6 h emission budgets. 2) We assign no temporal correlation of prior uncertainties between the different 6h time windows. The data selection criteria of the assimilated CO_2 observations and the assignments of the prior flux uncertainties of the reference inversion are shown in Table S1. In addition, we also conducted a series of sensitivity tests to investigate how the inverse estimates respond to changes in various setups of the inversion system (Table S1). This inversion ensemble was composed of 5 tests of the selection criteria of the assimilated CO_2 observations, and 5 tests of the uncertainties and the temporal correlations of the prior emissions.

3 Results

3.1 Daily emission estimates

Statistical comparisons between the assimilated modeled and measured CO_2 concentration gradients before and after flux optimizations are shown in Figure S5. In general, the inversion leads to an overall improvement in the representation of observations, both for the morning period (8-11 UTC) (Figure S5c) and the afternoon period (12-17 UTC) (Figure S5d). The mean bias errors (MBE) are reduced from -0.85 to -0.29 ppm in the morning and from -1.16 to -0.55 ppm in the afternoon after the inversion. The selected morning CO_2 gradients correspond to ~24.5% (5168 over 21091) of the total assimilated observation gradients.

Figure ~~2~~3 compares the estimates from the reference inversion, which assimilates the daytime (8-17 UTC) CO_2 concentration gradients, to the estimates from the two sensitivity tests that only use morning (8-11 UTC) or afternoon (12-17 UTC) CO_2 data respectively. Here, we mainly focus on the Greater Paris region (Figure 1) where the fossil fuel CO_2 emissions can be well constrained from our observation network. Figure ~~2~~3 shows the average prior and posterior fossil fuel CO_2 emission estimates together with their associated uncertainties over the 6-year period spanning January 2016 to December 2022, for the four 6 h time windows and every day of the week. The time series of the daily prior and posterior fossil fuel CO_2 emissions are shown in Figure ~~3~~4. The reference inversion (Figure ~~2b~~3b) mainly imposes a direct constraint on the fossil fuel fluxes for the two 6 h windows of the day (6-11 UTC and 12-17 UTC), while having little constraint on nighttime emissions (0-5 UTC and 18-23 UTC). This is because the assimilated daytime CO_2 concentrations are mainly sensitive to the emissions from the morning and afternoon periods. The inversion increases the average posterior emissions per day of the week by around 9~16% and 13~23% with uncertainty reductions of 14~21% and 15~21% for the 6-11 UTC and 12-17 UTC time windows respectively. The assimilation of only afternoon CO_2 data (Figure ~~2d~~3d) has similar retrieved emissions but with a smaller uncertainty reduction especially for the 6-11 UTC period compared to the reference one which assimilates morning data. Even though we assimilate a relatively small number of morning CO_2 data (Figure ~~2c~~3c), such a change still leads to a 11~16% uncertainty reduction compared to a priori of the morning fossil fuel emissions (Figure ~~2c~~3c).

The inversion on average reduces the uncertainty in the daily fossil fuel CO_2 emission estimates (Figure ~~3a~~4a) from ~31% (prior) down to ~24%±4.5% (posterior) (a range of 2.5%~11.5% uncertainty reduction) over the Greater Paris region. On the contrary,

CO_2 emissions over the rest of IdF region (Figure S6) after the inversion remain close to their prior values due to insufficient observational constraints. The inverse CO_2 emissions show a fairly good agreement with the prior estimate with a Pearson correlation coefficient (R) of 0.91, which indicates that the Origins.earth near-real-time inventory could already capture relatively well some timely emission variations that are closely related to meteorological effects and human activities. For instance, the lower emissions in February 2020 appears to be mainly due to weather conditions, with a mild winter leading to lower demand for heating (Météo-France climate bulletin, 2020). A decrease of the daily CO_2 emissions is observed in July and August due to a reduction in traffic emissions during the summer holidays. It can also be seen that the daily fossil fuel CO_2 emissions dropped by more than 30% in the second half of March 2020, when the strict COVID-19 lockdown measures were adopted. In general, the inverse CO_2 emissions exhibit a larger daily variability compared to the prior. On the one hand, the temporal profiles used in the inventory rely on some degree of interpolation, proxy data and theoretical assumptions that can smooth out some temporal variability. On the other hand, the posterior daily variability represents both the actual variability in emissions caused by human activities and the sources of uncertainty in the inverse modeling system, especially the transport model errors.

3.2 Monthly emission estimates

Figure ~~4a~~5a shows the posterior estimate of the monthly fossil fuel CO_2 emissions over the Greater Paris region derived through a temporal aggregation of the four 6 h period results. Results for the rest of IdF region are given in Figure S7. The inversion tends to increase the annual fossil fuel emissions by 2~6% with respect to the prior estimates for each of the years 2016 to 2021. It demonstrates the consistency of the measurement constraint on inverse fossil fuel CO_2 emissions over time. It is important to note that the inversions for the years 2016 and 2017 were carried out with the prior emissions from the 2018 Origins.earth inventory, making the inverse emission changes mainly rely on the assimilated CO_2 observations. With the same prior emissions for 2017 and 2018, the inversion leads to an emission reduction by 0.6% over the Greater Paris region from 2017 to 2018, which is consistent with the general trend towards a decrease in emission.

Figure ~~4b~~5b shows the relative difference between the posterior and prior fossil fuel CO_2 emissions corresponding to the different inversion setups (e.g., prior errors and correlation length). It is worth noting that the optimized monthly emissions are very similar across the six years from 2016 to 2021. More precisely, the inversion consistently points to an average 10% increase in fossil fuel emissions in winter months compared to the prior (January to March). Further, the inverse emissions show significantly higher values (>20%) with respect to the prior during the spring period (especially in May and June). In contrast, minor differences between the prior and posterior estimates are observed for the rest of the year. The ensemble of posterior fluxes, as represented by the spread of the minimum and maximum values among multiple inversions, provide an estimate of the variability introduced by a wide range of inversion setups. Even though these sensitivity tests may not represent the full potential range of uncertainties in the posterior fluxes, they still give us a certain degree of confidence in the inversion results because these variabilities are mostly smaller than the posterior-prior emission differences and the emissions uncertainties.

We then conducted a series of analyses to investigate the potential explanations for the adjustments to the prior fluxes made by the inversion. First, we infer that the seasonal variability in flux adjustments is not caused by biases in the atmospheric transport model. This is because the model-observation misfits in wind speed exhibit a relatively constant pattern throughout a year without a pronounced seasonality (Figure S8). Second, the 10% increase in fossil fuel CO_2 emissions during the winter months (January to March) could be due to an underestimation of the residential emissions in the Origins.earth inventory. The temporal profiles of the Origins.earth residential emissions are based on a proxy quantity derived from real-time domestic gas consumption data (Text ~~S4~~S3). Whereas in reality, this seasonal cycle in the prior emissions may underestimate wintertime energy demands from other

fuel types, especially for the petroleum and wood burning in the suburban residential areas (Figure S9). Notably, the estimated monthly emissions are ~20% larger compared to the prior estimates from April to June. Part of the adjustments of emissions could be due to an underestimation of the biogenic fluxes from the VPRM model (Text ~~S5~~S4). Figure S11 shows an obvious discrepancy between the VPRM simulated hourly biogenic flux (net ecosystem exchange, NEE) and the eddy flux measurements, especially during the growing season, at the Grignon cropland station located at around 40 km west of Paris center (Figure S10). The model-observation comparison of the vertical differences in CO_2 concentrations at the SAC station (15 m and 100 m above ground level) shows that the contribution of the nighttime biogenic respiration to the CO_2 concentration could also be a potential source of modeling errors during the growing season (Lian et al., 2021).

3.3 Annual emission estimates

Verification of annual emission totals and tracking emission trends over time using multiple methods constitutes an indication of the reliability of inverse emissions estimates. Moreover, given the potential impact of atmospheric transport errors on the emission estimates, and assuming that the model errors do not change statistically over time, the emission trends are expected to be less sensitive to model biases than the emissions estimates. The inter-annual variations are a critical metric to assess the effectiveness of the CO_2 mitigation efforts. Figure ~~5~~6 shows the multiyear trend in the annual total fossil fuel CO_2 emissions over the IdF region for the period 2005-2021. The prior and inverse emissions are compared to multiple inventory datasets. The interannual variation in fossil fuel CO_2 emissions indicates a decreasing trend over the IdF region during the 2005-2021 period using the Mann-Kendall (MK) trend test at 5% level of significance (p-values (0.0001) < 0.05). According to the TNO 6km inventory, this is mainly linked to the emission reductions in the residential and industry sectors, and further resulted from a decrease in coal use, an improvement in energy efficiency and building renovation. The inverse annual fossil fuel CO_2 emissions have been declining at a rate of ~2%±0.6% per year over the four-year period from 2016 to ~~2019~~2021 (MK test p-values (0.02) < 0.05). In 2020, the COVID-19 pandemic and the continued levels of restrictions in place resulted in a dramatic decline in human activity. Our inversion results indicate a ~13% (12-14%) reduction in the annual emissions in 2020 compared to 2019, which is 2% (1-3%) larger than the prior estimate based on the Origins.earth inventory (11%). The inverse annual emissions in 2021 rose by ~~~about 5.2%±14.2% to 34.3±2.3 $MtCO_2$ compared with 2020~~, (32.6±2.2 $MtCO_2$),~~ but still remains ~~7.~~ 8~~% below~~.0%±12.6% compared with the pre-COVID-19 level in 2019~~.~~ (37.3±2.6 $MtCO_2$).

The aggregated annual fossil fuel CO_2 emissions obtained with the inversion are on average higher by ~5% for each year compared to the prior estimates from the Origins.earth inventory. Our inversion results are in agreement with the TNO 1km inventory in the whole city-scale fossil fuel CO_2 estimates for the years 2017 and 2018, while they are approximately 8.6%, 3.6% and 3.1% higher than those estimated by Carbon Monitor Cities for the years 2019, 2020 and 2021, respectively. In 2018, the optimized emission is 38.1±2.6 $MtCO_2$. It is around 3.3, 2.7 and 0.8 $MtCO_2$ higher than that from AirParif, TNO 6 km and TNO 1km inventory respectively. Generally, the agreement among the various estimates of the annual fossil fuel CO_2 emission over the IdF region is within 10%, demonstrating robust emission estimates at the city scale through a combination of up-to-date inventories, atmospheric modeling, and observations. It also provides evidence for a continuous and timely monitoring of urban fossil fuel CO_2 emission trends toward the reduction targets to achieve carbon neutrality.

4 Conclusions and discussions

This study shows the capacity of our city-scale inversion system, with a state-of-the-art inventory and high-precision continuous CO_2 measurements, for a timely and effective monitoring of urban fossil fuel CO_2 emissions over a long-term time period from 2016 to 2021. Our results indicate a decreasing trend in the annual CO_2 emissions over the IdF region with an amplitude of ~2%±0.6% per year at 5% level of significance. The comparison of both prior and posterior annual emissions with independent estimates from other inventory datasets shows a less than 10% difference, which a satisfying target in terms of emission trend detection and verification for Paris to support its emissions-mitigation measures and related policy (Wu et al., 2016). In practice, few cities have such a high-resolution near-real-time local inventory like Paris. Through using the same annual total emission as a prior for the year 2016-2018, the posterior emissions exhibit an emission ~~reduction~~change by ~~~~about -3%±13.8% over the IdF region when comparing the year 2016 with 2018. This demonstrates the ability of the inversion system to detect emission changes based on CO_2 measurements, independent of the information provided by the prior inventory. In addition to the afternoon CO_2 measurements that are commonly used in CO_2 inversion system, the assimilation of morning CO_2 data when the ABL heights are well reproduced by the model could lead to an additional 11~16% uncertainty reduction of the morning fossil fuel emissions. But it is worth pointing out that the selection of morning CO_2 observations only for moderate to high wind speeds might reduce the observational constraint on the emissions in stable weather periods.

The uncertainties in the posterior estimates of CO_2 emissions are caused to a certain extent by errors in the spatio-temporal distribution of emissions at scales finer than the targeted ones. The present inversion system mainly controls the city-scale fossil fuel CO_2 emissions, but not the finer resolution in space. We thus further conducted a sensitivity inversion test using the TNO 1km inventory as a priori as an alternative to the Origins.earth dataset for 2018. The other parameters were kept identical to the reference inversion configuration. The TNO inventory indicates more fossil fuel CO_2 emissions concentrated within the Paris inner city compared to the Origins.earth dataset (Figure S12). The inversion was able to spatially differentiate between the Paris city center and the Greater Paris region (excluding Paris), correcting the respective emissions differently (Figure S13). The posterior fossil fuel CO_2 emissions from the Paris city center were adjusted more upward with Origins.earth than TNO, while those from the rest of Greater Paris region were corrected at a similar magnitude between Origins.earth and TNO. One can hope that a spatially explicit inversion system would allow to solve for the spatial distribution of urban emissions at the grid scale (Lauvaux et al., 2016). However, this will need additional information to determine the spatial correlation length of the inventory uncertainty or a high-density observation network to constrain the emissions from a large part of the city (Nalini et al., 2022).

Improvements in urban ecosystem modeling and monitoring for a precise accounting of urban biomass in the estimates of CO_2 fluxes is a relatively recent endeavor. Focusing on the Paris urban area, two limitations of this study have been acknowledged and are considered worthy of further investigation. Firstly, due to the coarse-resolution SYNMAP land use (1 km) data (Jung et al., 2006) and the MODIS satellite-derived vegetation indices (500m) used for the VPRM model, the simulated biogenic fluxes in Paris in this study are almost zero except for a few grid cells containing two big parks that are located in the eastern and western outskirts of the Paris city respectively. While in reality, there are still a number of green space and pervious landscaped areas unevenly distributed in the city of Paris that need to be considered with a fine-scale (sub-kilometer) model. Secondly, there is a lack of detailed evaluation of the Paris-VPRM model since no eddy covariance measurement is available within Paris and its surroundings yet. Our analyses indicate that the actual biogenic fluxes within the IdF region may have a recognizable influence on the measured CO_2 concentration gradients, whereas these biosphere signals are not well reproduced by the VPRM model. These discrepancies question the validity of the assumption that the signature of the local biogenic fluxes is not significant compared with that of the fossil fuel emissions in the measured gradients. Even though we have scaled up the prescribed observation errors

to account for this possible large model bias in the biogenic fluxes and thereby to reduce its interference in the inverse fossil fuel emissions, the results may still be inevitably hampered. This study highlights the need for an in-depth analysis of the seasonal and daily variations of the biogenic fluxes within the IdF region, especially during the cropland growing season. This could be achieved by improving the default VPRM model with a modified gross primary production and ecosystem respiration equations, domain-specific optimized parameters, high-resolution input datasets and high-quality diagnostic ~~phenology41~~phenology. In addition, measurements of carbon isotopes (^{14}C, ^{13}C) and tracers co-emitted with CO_2 (e.g., CO, NO_x, VOCs) could also be used to separate the contributions from fossil fuel and biogenic components to the total CO_2 concentrations, which would be beneficial for the optimization of sectoral CO_2 fluxes.

Author contribution

JL, TL and PC designed the study. JL did the coding and implementation of the research. JL, TL, PC, FMB, GB, HU, MR and IA contributed to the analysis and interpretation of the results. MR, OL and MC coordinated scientifically the development of CO_2 measurement stations and ensured the calibration of the dataset. SK and MH processed the observed ABL data and gave precious advice on the model-data evaluation. HU provided the Origins.earth inventory, OS and OP provided the AirParif emission estimates, HD and SD provided the TNO inventory, they all provided valuable feedback and opinions on the multiple dataset comparisons in section 3.3. JL prepared the manuscript with contributions and suggestions from all authors.

Code/Data availability

The hourly averaged CO_2 data measured at 7 in situ stations are available on request from Michel Ramonet (michel.ramonet@lsce.ipsl.fr).

The observed ABL height data are available on request from Simone Kotthaus (simone.kotthaus@ipsl.polytechnique.fr)

The Origins.earth CO_2 inventories are available on request from Hervé Utard (herve.utard@origins.earth).

The TNO CO_2 inventories are available on request from Hugo Anne Denier van der Gon (hugo.deniervandergon@tno.nl).

The ODIAC fossil fuel emission dataset was downloaded from https://db.cger.nies.go.jp/dataset/ODIAC/.

The Carbon Monitor Cities dataset is available at https://cities.carbonmonitor.org/.

The eddy covariance measurements were downloaded from the ICOS (https://doi.org/10.18160/2G60-ZHAK).

Competing interests

The authors have no competing interests to declare.

Acknowledgements

The authors would like to thank SUEZ Group ~~and~~, La Ville de Paris and ICOS Cities for the support of this study. Thanks to Marc Jamous at CDS, to the IPSL QUALAIR platform team and to Cristelle Cailteau-Fischbach (LATMOS/IPSL) at JUS, and to LSCE/RAMCES technical staff for the maintenance of the CO_2 monitoring network. Thanks also to Pauline Buysse, Jérémie Depuydt, Daniel Berveiller and Nicolas Delpierre for providing the eddy covariance flux measurements at Grignon and Fontainebleau (Barbeau) ecosystem sites. We thank Xiaobo Yang and Anna Agusti-Panareda from ECMWF for providing the

near-real-time (NRT) CAMS CO_2 dataset. We also thank Elise Potier for her help in processing the TNO inventory. We thank the technical and IT staff at the SIRTA observatory for operation of the ALC. We thank Melania Van Hove and the AERIS-ESPRI data center for supporting the MLH product retrieval.

Financial support

The authors have received funding from the ICOS Cities, aka Pilot Applications in Urban Landscapes - Towards integrated city observatories for greenhouse gases (PAUL) project by the European Union's Horizon 2020 research and innovation program under grant agreement NO.101037319. Thomas Lauvaux was supported by the project CIUDAD (Make Our Planet Great Again program) and the Chair Fellowship CASAL (French Ministry of Research - CNRS).

References

AIRPARIF: Bilan des émissions de polluants atmosphériques et de gaz à effet de serre en Île-de-France pour l'année 2010 et historique 2000/2005, 2013.

Bréon, F. M., Broquet, G., Puygrenier, V., Chevallier, F., Xueref-Remy, I., Ramonet, M., Dieudonné, E., Lopez, M., Schmidt, M., Perrussel, O., and Ciais, P.: An attempt at estimating Paris area CO_2 emissions from atmospheric concentration measurements. Atmospheric Chemistry and Physics, 15(4): 1707-1724, 2015.

Bulletin Climatique Météo-France, mensuel sur la France DÉCEMBRE 2016. https://donneespubliques.meteofrance.fr/donnees_libres/bulletins/BCM/201612.pdf. (last access: November 2022).

Bulletin Climatique Météo-France, mensuel sur la France JANVIER 2017. https://donneespubliques.meteofrance.fr/donnees_libres/bulletins/BCM/201701.pdf. (last access: November 2022).

Bulletin Climatique Météo-France, mensuel régional Ile de France FÉVRIER 2020. https://donneespubliques.meteofrance.fr/donnees_libres/bulletins/BCMR/BCMR_08_202002.pdf. (last access: November 2022).

Ciais, P., Rayner, P., Chevallier, F., Bousquet, P., Logan, M., Peylin, P., and Ramonet, M.: Atmospheric inversions for estimating CO_2 fluxes: methods and perspectives, Clim. Change, 103, 69-92, https://doi.org/10.1007/s10584-010-9909-3, 2010.

Davis, K. J., Deng, A., Lauvaux, T., Miles, N. L., Richardson, S. J., Sarmiento, D. P., Gurney, K. R., Hardesty, R. M., Bonin, T. A., Brewer, W. A., Lamb, B. K., Shepson, P. B., Harvey, R. M., Cambaliza, M. O., Sweeney, C., Turnbull, J. C., Whetstone, J., and Karion, A.: The Indianapolis Flux Experiment (INFLUX): A test-bed for developing urban greenhouse gas emission measurements. Elem Sci Anth, 5:21, 2017.

Dellaert S., Super I., Visschedijk A., Denier van der Gon H.A.C.: High resolution scenarios of CO_2 and CO emissions. https://www.che-project.eu/sites/default/files/2019-05/CHE-D4-2-V1-0.pdf, 2019.

Deng, A., Lauvaux, T., Davis, K. J., Gaudet, B. J., Miles, N., Richardson, S. J., Wu, K., Sarmiento, D. P., Hardesty, R. M., Bonin, T. A., Brewer, W. A., and Gurney, K. R.: Toward reduced transport errors in a high resolution urban CO_2 inversion system. Elem Sci Anth, 5, 20, 2017.

Denier van der Gon H.A.C., Dellaert S., Super I., Kuenen J., Visschedijk A.: TNO GHGco emission inventory v3.0: final high resolution emission data 2005-2018. https://verify.lsce.ipsl.fr/images/PublicDeliverables/VERIFY_D2_3_TNO_v1.pdf, 2021.

Greater London Authority (GLA): London Atmospheric Emissions Inventory (LAEI) 2019, available at: https://airdrive-secure.s3-eu-west-1.amazonaws.com/london/dataset/london-atmospheric-emissions-inventory--laei--2019/2022-02-03T13%3A13%3A03/LAEI%202019%20Summary%20Note%20FINAL%20V2.pdf?X-Amz-Algorithm=AWS4-HMAC-SHA256&X-Amz-Credential=AKIAJJDIMAIVZJDICKHA%2F20221124%2Feu-west-1%2Fs3%2Faws4_request&X-Amz-Date=20221124T123620Z&X-Amz-Expires=300&X-Amz-Signature=b02b10e7fa688e0b2e7a70b351a8144032e56007048138b71710feebbcbc2e5e&X-Amz-SignedHeaders=host (last access: November 2022), 2021.

Grell, G. A., Peckham, S. E., Schmitz, R., McKeen, S. A., Frost, G., Skamarock, W. C., and Eder, B.: Fully coupled "online" chemistry within the WRF model. Atmospheric Environment, 39, 6957-6975, 2005.

Gourdji S M, Karion A, Lopez-Coto I, et al. A modified Vegetation Photosynthesis and Respiration Model (VPRM) for the eastern USA and Canada, evaluated with comparison to atmospheric observations and other biospheric models. Journal of Geophysical Research: Biogeosciences, 2022, 127(1): e2021JG006290.

Gurney, K. R., Patarasuk, R., Liang, J., Song, Y., O'Keeffe, D., Rao, P., Whetstone, J. R., Duren, R. M., Eldering, A., and Miller, C.: The Hestia fossil fuel CO_2 emissions data product for the Los Angeles megacity (Hestia-LA), Earth Syst. Sci. Data, 11, 1309-1335, 2019.

Gurney, K. R., Liang, J., Roest, G., Song, Y., Mueller, K., and Lauvaux, T.: Under-reporting of greenhouse gas emissions in US cities. Nature Communications, 12(1), 1–7. https://doi.org/10.1038/s41467-020-20871-0, 2021.

Haeffelin, M., Barthès, L., Bock, O., Boitel, C., Bony, S., Bouniol, D., Chepfer, H., Chiriaco, M., Cuesta, J., Delanoë, J., Drobinski, P., Dufresne, J.-L., Flamant, C., Grall, M., Hodzic, A., Hourdin, F., Lapouge, F., Lemaître, Y., Mathieu, A., Morille, Y., Naud, C., Noël, V., O'Hirok, W., Pelon, J., Pietras, C., Protat, A., Romand, B., Scialom, G., and Vautard, R.: SIRTA, a ground-based atmospheric observatory for cloud and aerosol research, Ann. Geophys., 23, 253–275, https://doi.org/10.5194/angeo-23-253-2005, 2005.

Hall, B. D., Crotwell, A. M., Kitzis, D. R., Mefford, T., Miller, B. R., Schibig, M. F., and Tans, P. P.: Revision of the World Meteorological Organization Global Atmosphere Watch (WMO/GAW) CO_2 calibration scale, Atmos. Meas. Tech., 14, 3015–3032, https://doi.org/10.5194/amt-14-3015-2021, 2021.

Huo, D., Huang, X., Dou, X. et al. Carbon Monitor Cities near-real-time daily estimates of CO_2 emissions from 1500 cities worldwide. Sci Data 9, 533. https://doi.org/10.1038/s41597-022-01657-z, 2022.

Jung, M., Henkel, K., Herold, M., and Churkina, G.: Exploiting synergies of global land cover products for carbon cycle modeling. Remote Sensing of Environment, 101, 534-553, 2006.

Karion, A., Callahan, W., Stock, M., Prinzivalli, S., Verhulst, K. R., Kim, J., Salameh, P. K., Lopez-Coto, I., and Whetstone, J.: Greenhouse gas observations from the Northeast Corridor tower network, Earth Syst. Sci. Data, 12, 699–717, https://doi.org/10.5194/essd-12-699-2020, 2020.

Kotthaus, S., Haeffelin, M., Drouin, M.-A., Dupont, J.-C., Grimmond, S., Haefele, A., Hervo, M., Poltera, Y., Wiegner, M.: Tailored Algorithms for the Detection of the Atmospheric Boundary Layer Height from Common Automatic Lidars and Ceilometers (ALC). Remote Sensing. 12(19):3259, 2020.

Kretschmer, R., Gerbig, C., Karstens, U., and Koch, F. T.: Error characterization of CO_2 vertical mixing in the atmospheric transport model WRF-VPRM. Atmospheric Chemistry and Physics, 12(5), 2441-2458, 2012.

Lauvaux, T., Miles, N. L., Deng, A., Richardson, S. J., Cambaliza, M. O., Davis, K. J., Gaudet, B., Gurney, K. R., Huang, J., O'Keeffe, D., Song, Y., Karion, A., Oda, T., Patarasuk, R., Sarmiento, D., Shepson, P., Sweeney, C., Turnbull, J., and Wu, K.: High-resolution atmospheric inversion of urban CO_2 emissions during the dormant season of the Indianapolis Flux Experiment (INFLUX). Journal of Geophysical Research: Atmospheres, 121(10): 5213-5236, 2016.

Lauvaux, T., Gurney, K. R., Miles, N. L., Davis, K. J., Richardson, S. J., Deng, A., Nathan, B. J., Oda, T., Wang, J. A., Hutyra, L., and Turnbull, J.: Policy-Relevant Assessment of Urban CO_2 Emissions, Environ. Sci. Technol., 54, 10237–10245, https://doi.org/10.1021/acs.est.0c00343, 2020.

Le Plan Climat de Paris. https://cdn.paris.fr/paris/2020/11/23/99f03e85e9f0d542fad72566520c578c.pdf. (last access: September 2022).

Lian, J., Bréon, F. M., Broquet, G., Zaccheo, T. S., Dobler, J., Ramonet, M., Staufer, J., Santaren, D., Xueref-Remy, I., and Ciais, P.: Analysis of temporal and spatial variability of atmospheric CO_2 concentration within Paris from the GreenLITE™ laser imaging experiment. Atmospheric Chemistry and Physics, 19, 13809-13825, 2019.

Lian, J., Bréon, F. M., Broquet, G., Lauvaux, T., Zheng, B., Ramonet, M., Xueref-Remy, I., Kotthaus, S., Haeffelin, M., and Ciais, P.: Sensitivity to the sources of uncertainties in the modeling of atmospheric CO_2 concentration within and in the vicinity of Paris, Atmos. Chem. Phys., 21, 10707–10726, https://doi.org/10.5194/acp-21-10707-2021, 2021.

Lian, J., Lauvaux, T., Utard, H., Broquet, G., Bréon, F.M., Ramonet, M., Laurent, O., Albarus, I., Cucchi, K., and Ciais, P.: Assessing the Effectiveness of an Urban CO_2 Monitoring Network over the Paris Region through the COVID-19 Lockdown Natural Experiment. Environmental Science & Technology, https://doi.org/10.1021/acs.est.1c04973, 2022.

Lopez, M., Schmidt, M., Delmotte, M., Colomb, A., Gros, V., Janssen, C., Lehman, S. J., Mondelain, D., Perrussel, O., Ramonet, M., Xueref-Remy, I., and Bousquet, P.: CO, NOx and 13CO2 as tracers for fossil fuel CO_2: results from a pilot study in Paris during winter 2010. Atmospheric Chemistry and Physics, 13, 7343-7358, 2013.

Mahadevan, P., Wofsy, S. C., Matross, D. M., Xiao, X., Dunn, A. L., Lin, J. C., Gerbig, C., Munger, J. W., Chow, V. Y., and Gottlieb, E. W.: A satellite-based biosphere parameterization for net ecosystem CO_2 exchange: Vegetation Photosynthesis and Respiration Model (VPRM). Global Biogeochemical Cycles, 22(2), 2008.

McKain, K., Wofsy, S. C., Nehrkorn, T., Eluszkiewicz, J., Ehleringer, J. R., and Stephens, B. B.: Assessment of ground-based atmospheric observations for verification of greenhouse gas emissions from an urban region. Proceedings of the National Academy of Sciences, 109(22): 8423-8428, 2012.

Mueller, K. L., Lauvaux, T., Gurney, K. R., Roest, G., Ghosh, S., Gourdji, S. M., Karion, A., DeCola, P., and Whetstone, J.: An emerging GHG estimation approach can help cities achieve their climate and sustainability goals, Environ. Res. Lett., 16, 084003, https://doi.org/10.1088/1748-9326/ac0f25, 2021.

Nalini, K., Lauvaux, T., Abdallah, C., Lian, J., Ciais, P., Utard, H., Laurent, O., and Ramonet, M.: High-resolution Lagrangian inverse modeling of CO_2 emissions over the Paris region during the first 2020 lockdown period. Journal of Geophysical Research: Atmospheres, 127, e2021JD036032, https://doi.org/10.1029/2021JD036032, 2022.

Nielsen-Gammon, J. W., Powell, C. L., Mahoney, M. J., Angevine, W. M., Senff, C. J., White, A., Berkowitz, C., Doran, C., and Knupp, K.: Multisensor estimation of mixing heights over a coastal city. Journal of Applied Meteorology and Climatology, 47(1): 27-43, 2008.

Oda, T., ~~Bun, R., Kinakh, V., Topylko, P., Halushchak, M., Marland, G., Lauvaux, T., Jonas, M.,~~ Maksyutov, S., ~~Nahorski, Z., Lesiv, M., Danylo, O.~~ and ~~Horabik-Pyzel,~~Andres, R. J.~~: Errors and uncertainties in~~: The Open-source Data Inventory for Anthropogenic CO_2, version 2016 (ODIAC2016): a global monthly fossil fuel CO_2 gridded ~~carbon dioxide emission inventory, Mitigation and Adaptation Strategies for Global Change~~emissions data product for tracer transport simulations and surface flux inversions, Earth Syst. Sci. Data, 10, 87–107, https://doi.org/10.~~1007/s11027-019-09877-2, 2019~~5194/essd-10-87-2018, 2018.

Sargent, M., Barrera, Y., Nehrkorn, T., Hutyra, L. R., Gately, C. K., Jones, T., McKain, K., Sweeney, C., Hegarty, J., Hardiman, B., Wang, J. A., and Wofsy, S. C.: Anthropogenic and biogenic CO_2 fluxes in the Boston urban region. Proceedings of the National Academy of Sciences, 115(29), 7491-7496, 2018.

Seto, K. C., Dhakal, S., Bigio, A., Blanco, H., Delgado, G. C., Dewar, D., Huang, L., Inaba, A., Kansal, A., Lwasa, S., McMahon, J., Müller, D. B., Murakami, J., Nagendra, H., and Ramaswami, A.: Human settlements, infrastructure and spatial planning, chap. 12, in: Climate Change 2014: Mitigation of Climate Change. IPCC Working Group III Contribution to AR5. Cambridge University Press, Cambridge, UK and New York, NY, USA, 2014.

Staufer, J., Broquet, G., Bréon, F.-M., Puygrenier, V., Chevallier, F., Xueref-Rémy, I., Dieudonné, E., Lopez, M., Schmidt, M., Ramonet, M., Perrussel, O., Lac, C., Wu, L., and Ciais, P.: The first 1-year-long estimate of the Paris region fossil fuel CO_2 emissions based on atmospheric inversion, Atmos. Chem. Phys., 16, 14703–14726, https://doi.org/10.5194/acp-16-14703-2016, 2016.

Tarantola A. Inverse problem theory and methods for model parameter estimation[M]. Society for industrial and applied mathematics, 2005.

Turner, A. J., Kim, J., Fitzmaurice, H., Newman, C., Worthington, K., Chan, K., Wooldridge, P. J., Köehler, P., Frankenberg, C., and Cohen, R. C.: Observed impacts of COVID-19 on urban CO_2 emissions. Geophysical Research Letters, 47(22), e2020GL090037. https://doi.org/10.1029/2020GL090037, 2020.

Vogel, F. R., Frey, M., Staufer, J., Hase, F., Broquet, G., Xueref-Remy, I., Chevallier, F., Ciais, P., Sha, M. K., Chelin, P., Jeseck, P., Janssen, C., Té, Y., Groß, J., Blumenstock, T., Tu, Q., and Orphal, J.: XCO_2 in an emission hot-spot region: the COCCON Paris campaign 2015, Atmospheric Chemistry and Physics, 19, 3271-3285, 2019.

Wu, L., Broquet, G., Ciais, P., Bellassen, V., Vogel, F., Chevallier, F., Xueref-Remy, I., and Wang, Y.: What would dense atmospheric observation networks bring to the quantification of city CO_2 emissions?, Atmospheric Chemistry and Physics, 16(12): 7743-7771, 2016.

Xueref-Remy, I., Dieudonné, E., Vuillemin, C., Lopez, M., Lac, C., Schmidt, M., Delmotte, M., Chevallier, F., Ravetta, F., Perrussel, O., Ciais, P., Bréon, F.-M., Broquet, G., Ramonet, M., Spain, T. G., and Ampe, C.: Diurnal, synoptic and seasonal variability of atmospheric CO_2 in the Paris megacity area. Atmospheric Chemistry and Physics, 18, 3335-3362, 2018.

Yadav, V., Ghosh, S., Mueller, K., Karion, A., Roest, G., Gourdji, S. M., Lopez-Coto, I., Gurney, K. R., Parazoo, N., Verhulst, K. R., Kim, J., Prinzivalli, S., Fain, C., Nehrkorn, T., Mountain, M., Keeling, R. F., Weiss, R. F., Duren, R., Miller, C. E., and Whetstone, J.: The impact of COVID - 19 on CO_2 emissions in the Los Angeles and Washington DC/Baltimore metropolitan areas. Geophysical Research Letters, 48(11), https://doi.org/10.1029/2021GL092744, 2021.

Wu, L., Broquet, G., Ciais, P., Bellassen, V., Vogel, F., Chevallier, F., Xueref-Remy, I., and Wang, Y.: What would dense atmospheric observation networks bring to the quantification of city CO_2 emissions?, Atmospheric Chemistry and Physics, 16(12): 7743-7771, 2016.

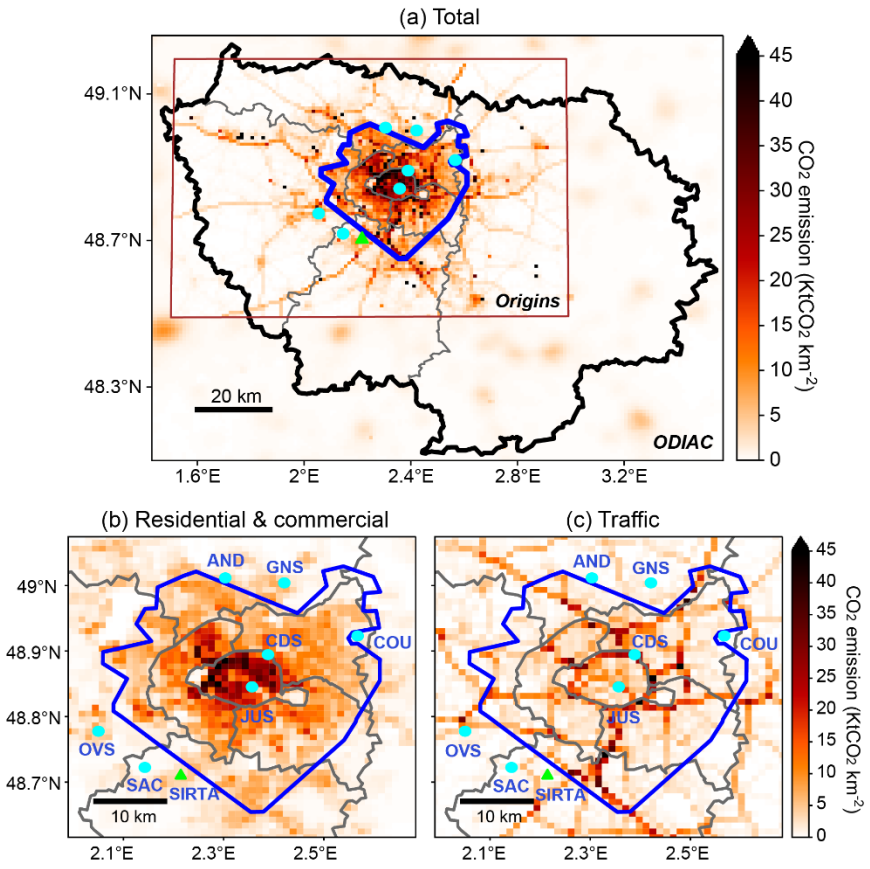

Figure 1: Distributions of annual (a) total fossil fuel, (b) residential and commercial, and (c) traffic CO_2 emissions for the year 2019 according to the Origins.earth inventory (brown rectangle) complemented by the ODIAC dataset. The seven in situ CO_2 measurement stations are shown in cyan circles. The location of the SIRTA observatory with ABL measurements is marked by a green triangle. The black bold line shows the administrative limits of the Île-de-France (IdF) region. In the inversion system, emissions over two emitting regions are optimized: the Greater Paris region (within blue line) and the rest of the IdF region.

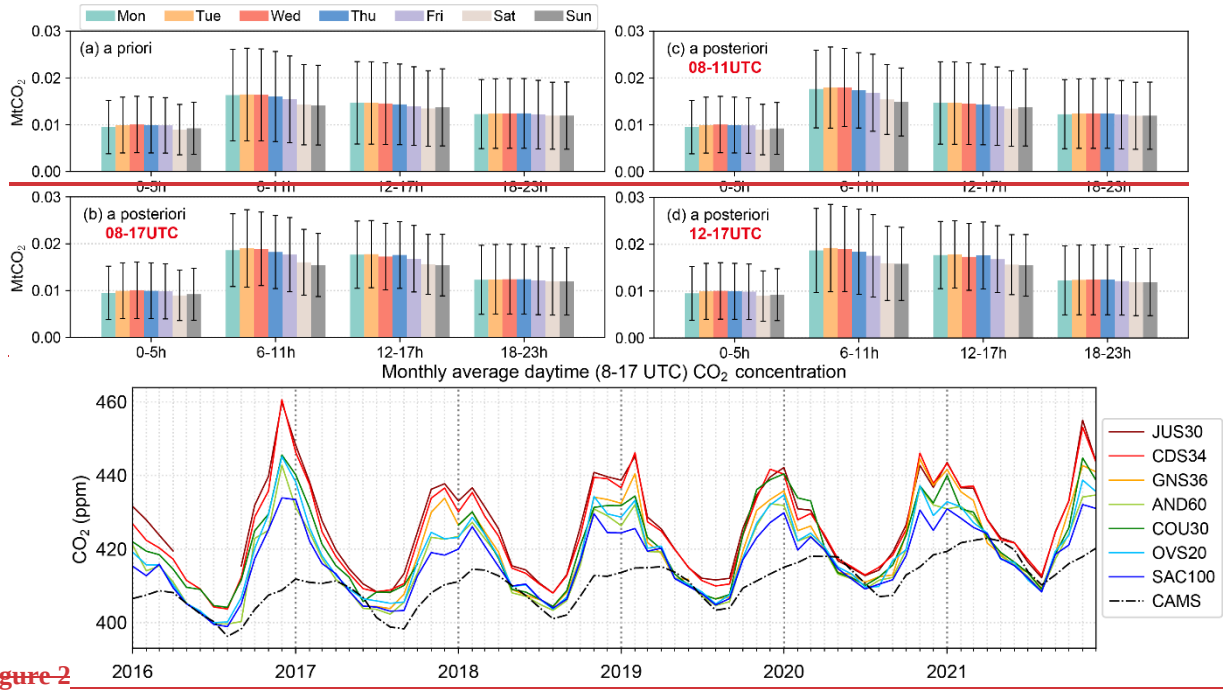

~~Figure 2~~

Figure 2: Monthly average daytime (8-17 UTC) observed CO_2 concentrations at seven in situ stations. The black dash line indicates the simulated background CO_2 concentration over Paris by WRF-Chem driven by the CAMS global atmospheric CO_2 dataset.

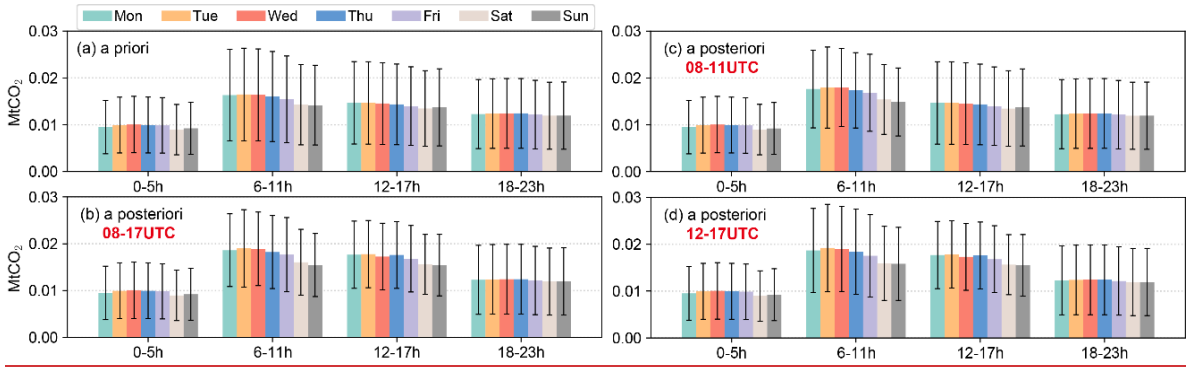

Figure 3: Average (a) prior and (b-d) posterior fossil fuel CO_2 emission estimates and their uncertainties over the Greater Paris region over the year 2016-2021, for the four 6-hour time windows and the days of the week. (b-d) present the posterior CO_2 estimates when assimilating (b) daytime (8-17 UTC), (c) morning (8-11 UTC) and (d) afternoon (12-17 UTC) selected CO_2 concentration observations, respectively.

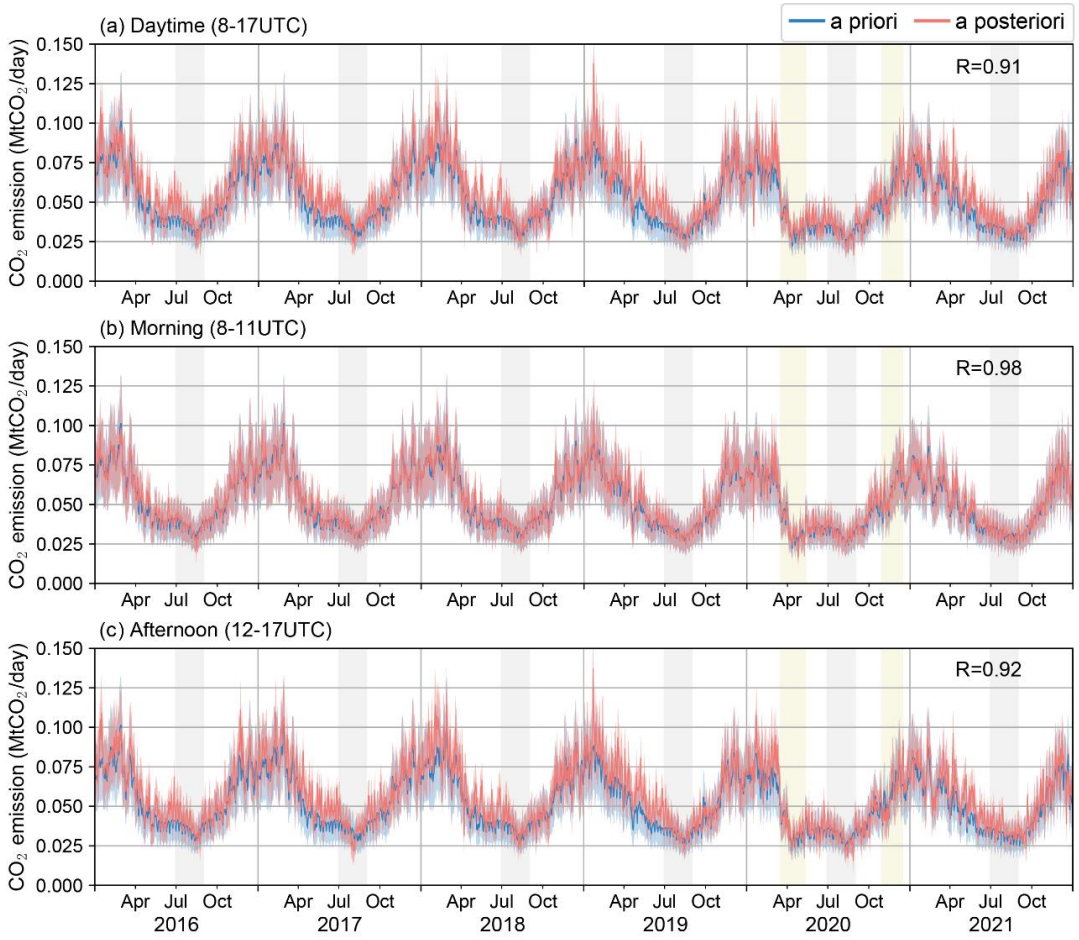

Figure ~~3~~4: Daily estimates of fossil fuel CO_2 emissions over the Greater Paris region when assimilating (a) daytime (8-17 UTC), (b) morning (8-11 UTC) and (c) afternoon (12-17 UTC) CO_2 concentration observations. The blue line and shading show the prior flux according to the Origins.earth inventory together with its assumed uncertainty. The pink and shading show the posterior estimates with their uncertainty ranges. The yellow shaded areas are the two COVID-19 lockdown periods in France. The grey shaded areas are the summer holidays of July and August.

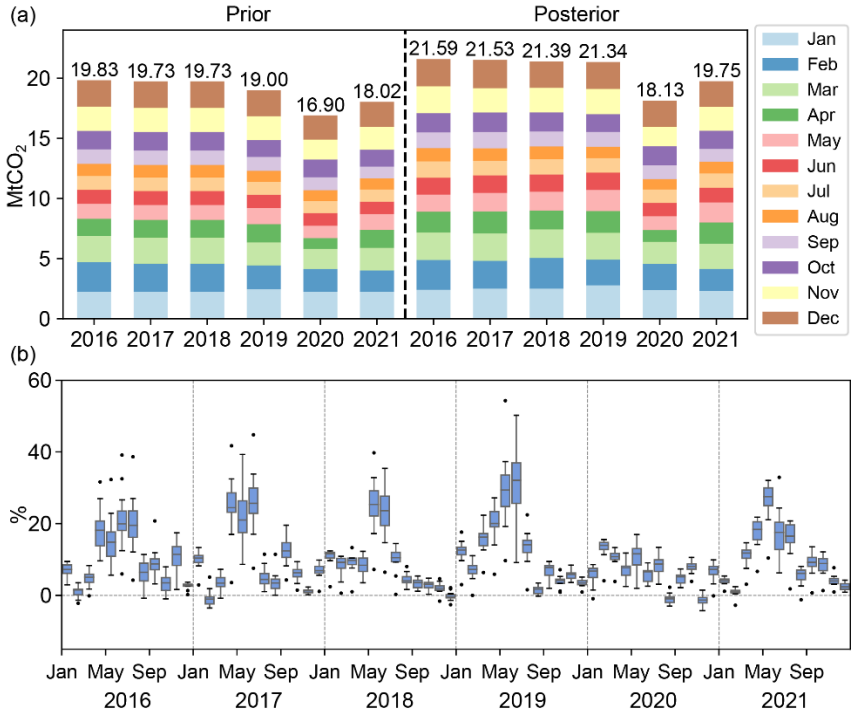

Figure 45: (a) Prior and posterior estimates of the monthly total fossil fuel CO_2 emission over the Greater Paris region. (b) the change of CO_2 emissions in percentage (posterior-prior)/prior. The boxplots are the posterior emissions from an ensemble of sensitivity tests of the inversion configuration. Note that the prior emission for 2016 is slightly higher than 2017 and 2018 since it is a leap year.

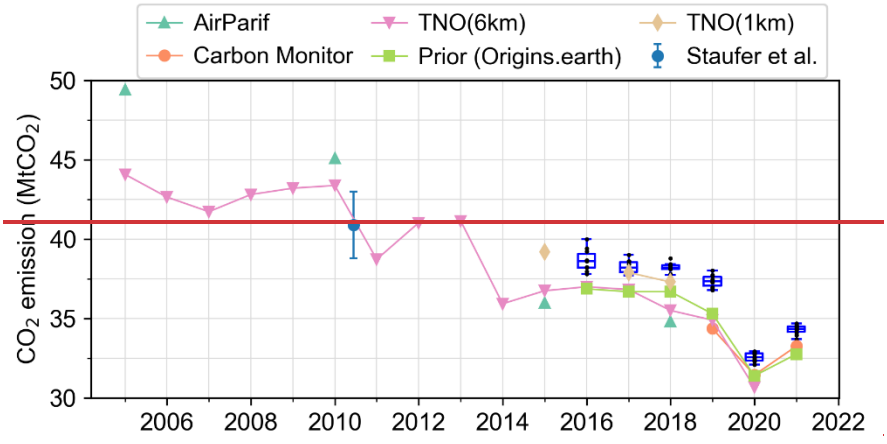

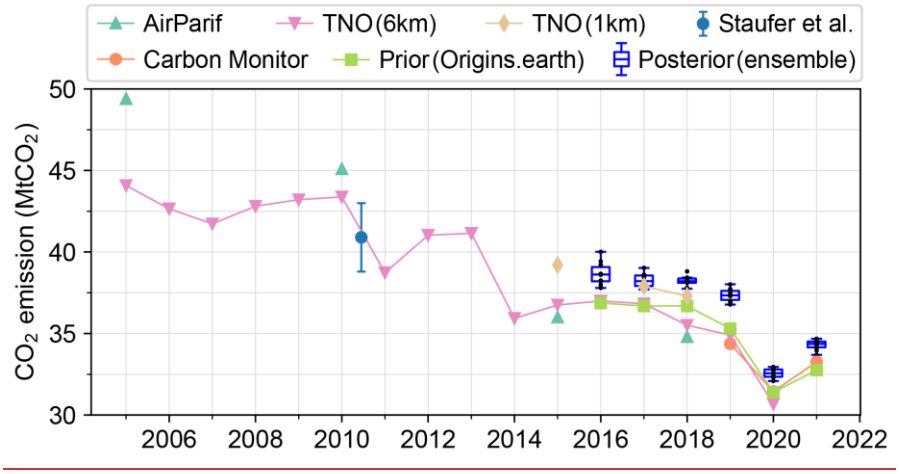

Figure ~~5~~6: Annual fossil fuel CO_2 emissions over the IdF region from 2005 to 2021. The blue boxplots present the distribution of posterior CO_2 emissions from an ensemble of sensitivity tests of the inversion configuration.

5

Supplement

Can we use atmospheric CO_2 measurements to verify emission trends reported by cities? Lessons from a six-year atmospheric inversion over Paris

Jinghui Lian[1,2], Thomas Lauvaux[3], Hervé Utard[1], François-Marie Bréon[2], Grégoire Broquet[2], Michel Ramonet[2], Olivier Laurent[2], Ivonne Albarus[1,2], Mali Chariot[2], Simone Kotthaus[4], Martial Haeffelin[4], Olivier Sanchez[5], Olivier Perrussel[5], Hugo Anne Denier van der Gon[6], Stijn Nicolaas Camiel Dellaert[6], and Philippe Ciais[2,7]

[1] Origins.earth, SUEZ Group, Tour CB21, 16 Place de l'Iris, 92040 Paris La Défense Cedex, France
[2] Laboratoire des Sciences du Climat et de l'Environnement (LSCE), IPSL, CEA-CNRS-UVSQ, Université Paris-Saclay, 91191 Gif sur Yvette Cedex, France
[3] Groupe de Spectrométrie Moléculaire et Atmosphérique (GSMA), Université de Reims-Champagne Ardenne, UMR CNRS 7331, Reims, France
[4] Institut Pierre Simon Laplace (IPSL), CNRS, École Polytechnique, Institut Polytechnique de Paris, 91128 Palaiseau Cedex, France
[5] AirParif, 7 rue Crillon, Paris, France
[6] Department of Climate, Air and Sustainability, TNO, P.O. Box 80015, 3508 TA Utrecht, Netherlands
[7] Climate and Atmosphere Research Center (CARE-C), The Cyprus Institute, 20 Konstantinou Kavafi Street, 2121, Nicosia, Cyprus

Correspondence to: Jinghui Lian (jinghui.lian@suez.com)

This PDF file includes:

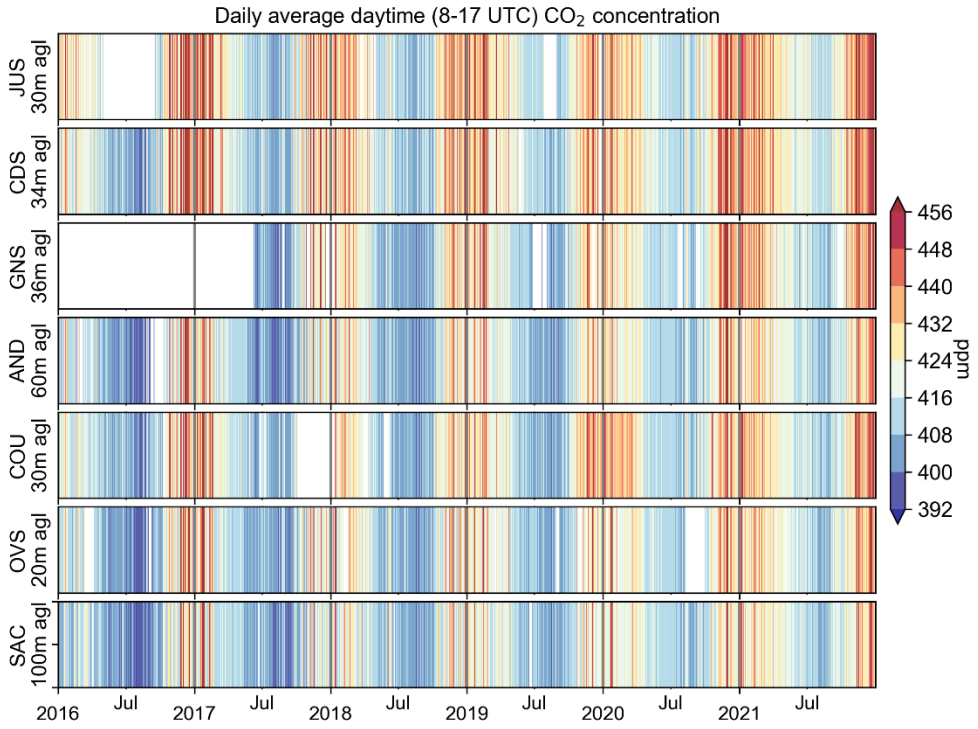

Figure S1. Daily average daytime (8-17 UTC) observed CO_2 concentrations from 2016 to 2021 at seven in situ stations within Paris and its surrounding areas, together with their respective heights above ground level of the air intake inlet.

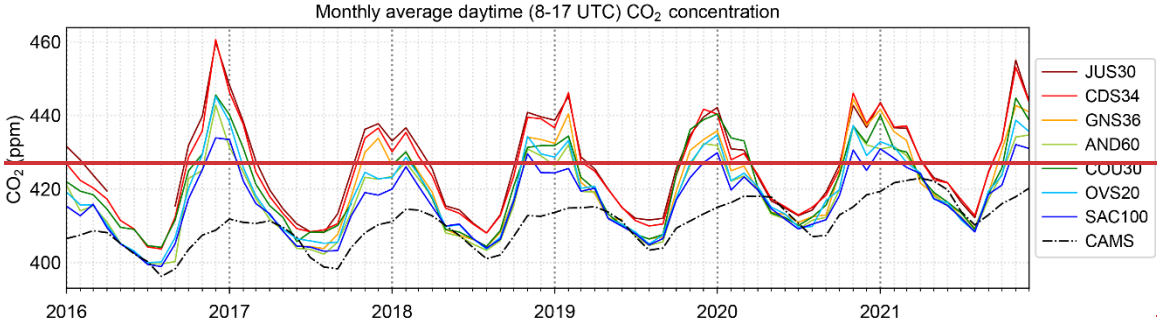

~~**Figure S2. Monthly average daytime (8-17 UTC) observed CO_2 concentrations at seven in situ stations. The black dash line indicates the simulated background CO_2 concentration over Paris by WRF-Chem driven by the CAMS global atmospheric CO_2 dataset.**~~

Text S1. Origins.earth fossil fuel CO_2 emission inventory

The Origins.earth inventory compilation method is mainly based on methodologies developed by Pôle National des Inventaires Territoriaux (PCIT, 2019), the body tasked by the French government to establish national guidelines for computing GHG emission inventories for local authorities. The near real-time high-resolution CO_2 emission maps are generated through the following two-step process. The first step involves the construction of gridded annual CO_2 emission datasets for different sectors for the base year 2018, which consists in spatializing geographically the intensity of annual emissions of the IdF region reported by the French climate agency (ROSE, https://www.roseidf.org/). Sector-specific spatial proxies (i.e., high spatial resolution French population census, CORINE Land Cover, locations of the thermal power stations, incinerators, and main emitting industries) are applied to allocate emissions to spatially resolved grids. The second step combines the annual sectorial emission maps with respective generic and/or measure-based (real activity data) temporal profiles. It combines the annual sectorial emission maps with respective generic and/or measure-based (real activity data) temporal profiles. For example, the on-road traffic emissions in the city of Paris are scaled using the real-time traffic count data from more than 3000 traffic measurement points. For the on-road traffic outside the Paris city, the temporal variations are assumed to follow the mean changes of the ones in the city. The temporal evolution of the residential emissions is estimated using the domestic gas consumption data from the SmartGRT database (https://smart.grtgaz.com/en/consommation). This proxy discards the specific temporal variations of other energy sources for the residential sector (e.g., petroleum, wood, coal), which may introduce additional uncertainties. Emissions from the tertiary, industry and energy are downscaled to hourly values based on the industrial gas consumption without SFM (Sites Fortement Modulés). Note that developing the near real-time CO_2 gridded emissions by sector at high-resolution is a relatively new endeavor. We continue to revise the methodology to further improve data quality.

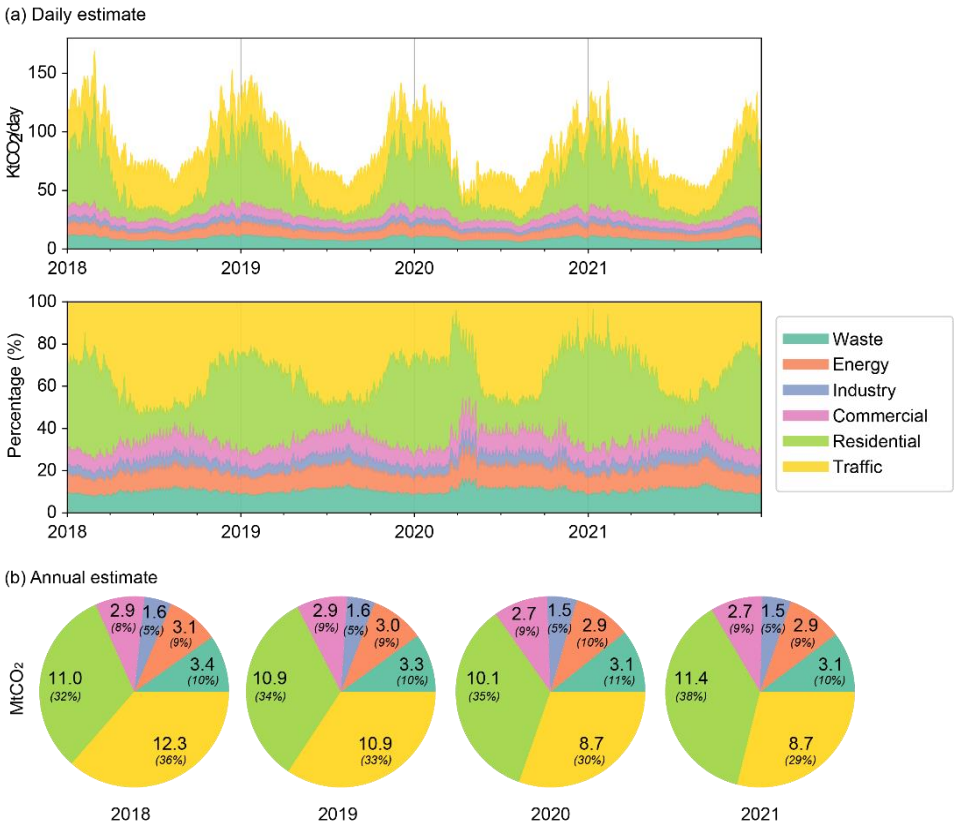

Figure S3S2. (a) Daily and (b) annual sectorial fossil fuel CO_2 emission estimates and their respective proportions from 2018 to 2021 according to the Origins.earth inventory.

Text S2. Evaluation of the observed and modeled ABL heights

In this study, we assume systematic differences between the thermodynamic and aerosol-based layer detection are negligible or in fact that the aerosol-based results provide a more suitable description for the dilution of near-surface CO_2 emissions, but it should be noted that these issues are subject to current research (Kotthaus et al. 2023).

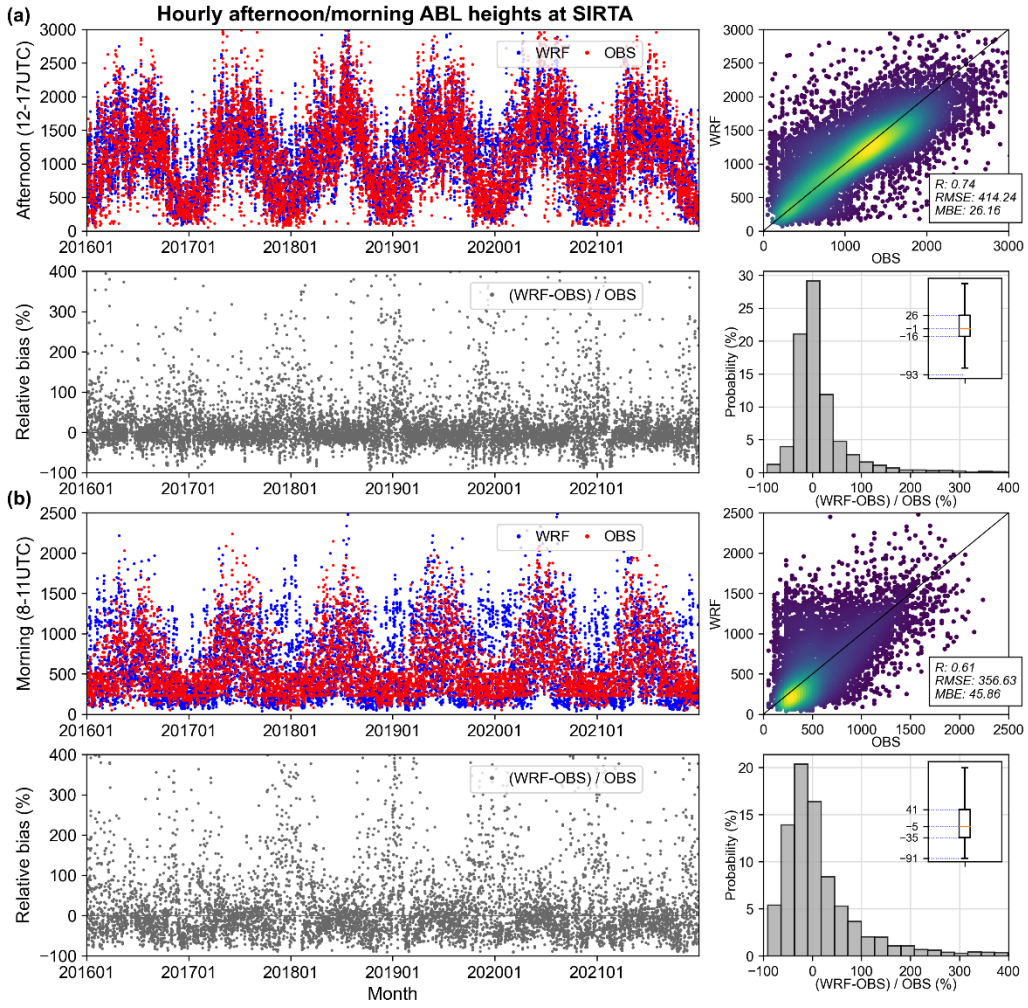

Figure ~~S4~~S3. Comparison of the observed and modeled hourly ABL heights at SIRTA station, both for the (a) afternoon (12-17 UTC) and (b) morning (8-11 UTC) period.

~~Text S3. Inversion configuration~~

~~The configuration of the atmospheric inversion system in this study are described in detail in Lian et al. (2022). It comprises the setup of the control vectors, the selection of the assimilated CO_2 observation gradients, the assignments of the observation error and the prior flux uncertainties. Only two minor modifications were made in this study in order to assess the impacts of morning CO_2 concentrations on the retrieved emissions: 1) Regarding the fossil fuel emissions, we assume a 60% relative uncertainty in the prior estimates of individual 6 h emission budgets. 2) We assign no temporal correlation of prior uncertainties between the different 6h time windows.~~

~~The data selection criteria of the assimilated CO_2 observations and the assignments of the prior flux uncertainties of the reference inversion are shown in Table S1. Similar as Lian et al. (2022), we also conducted a series of sensitivity tests to investigate how the inverse estimates respond to changes in various setups of the inversion system.~~

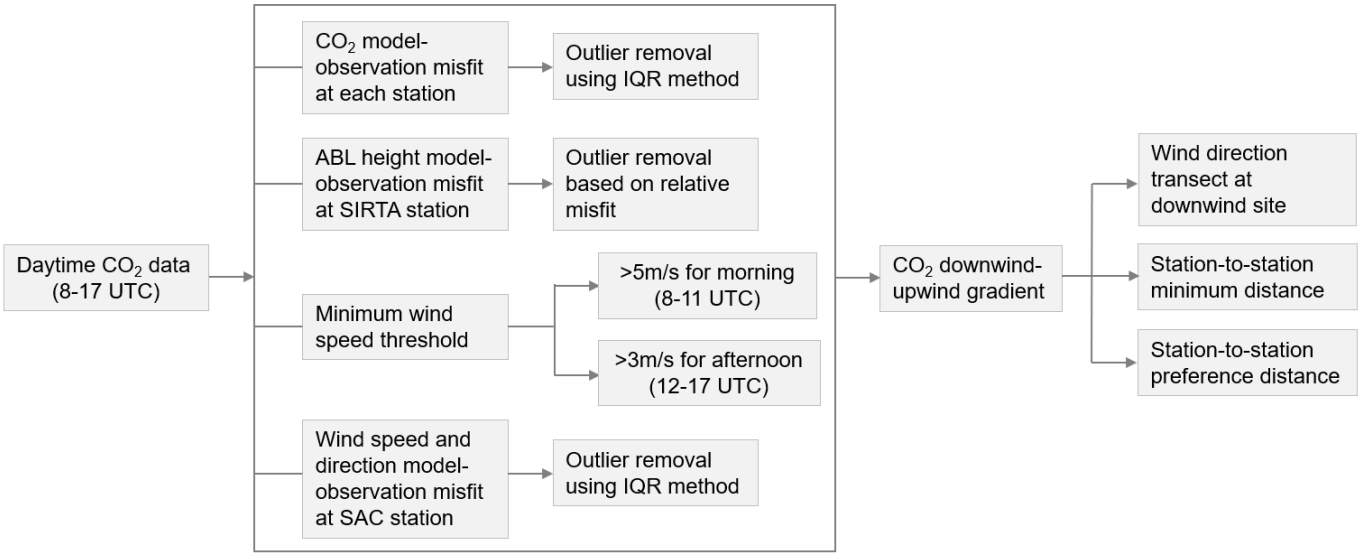

Figure S4. Roadmap for the selection of the assimilated CO_2 observation data into the inversion system

Table S1. Summary of inversion configurations used in this study, both for the reference inversion setup and for the sensitivity tests with changing one configuration at a time compared to the reference.

Category	Description	Reference inversion	Sensitivity test
Data selection criteria	Time period of the assimilated data	Daytime (8-17 UTC)	Morning (8-11 UTC) / Afternoon (12-17 UTC)
	Wind bias outlier based on an interquartile range (IQR) method	0.5	
	Minimum wind speed	3m/s	
	Wind direction transects	30°	20°
	Station-to-station minimum distance	10km	
	Station-to-station preference distance	32 km	20km / 40 km
Prior flux uncertainty	Day-to-day temporal correlation	1 day	4 days
	Uncertainty for 6h fossil fuel flux	60%	40% / 80%
	Uncertainty for daily biogenic flux	60%	40% / 100%

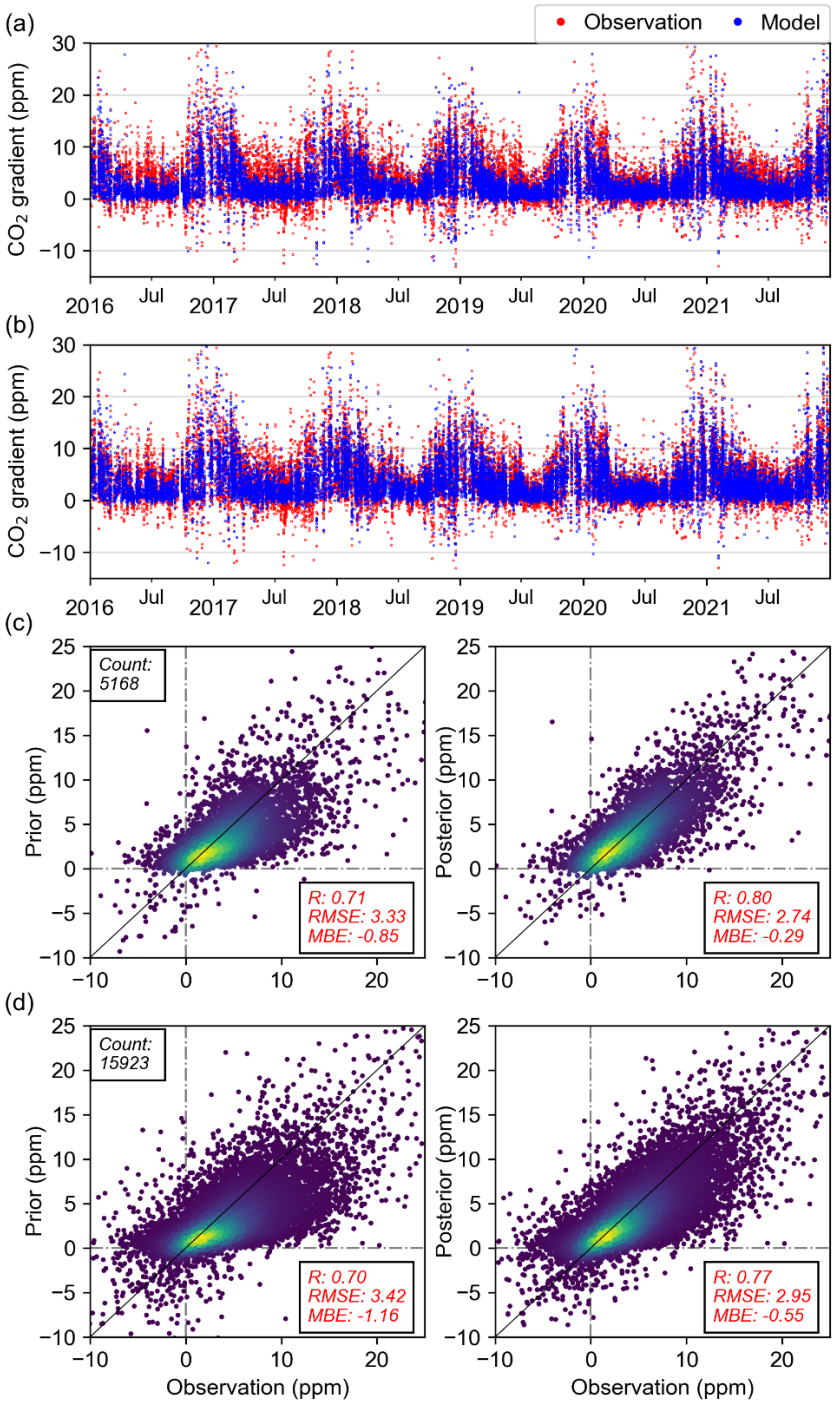

Figure S5. The assimilated hourly daytime CO_2 concentration gradients with (a) prior fluxes and (b) posterior fluxes against the observations from 2016 to 2021. Scatter plot of the assimilated observations and the corresponding simulated CO_2 concentration gradients using the prior fluxes and the posterior fluxes for the (c) morning 8-11 UTC and (d) afternoon 12-17 UTC period, respectively. The statistics of the coefficient correlation (R), root mean square error (RMSE) and mean bias error (MBE) of prior model-data misfit and posterior model-data misfit for the inversion are also provided in the figure.

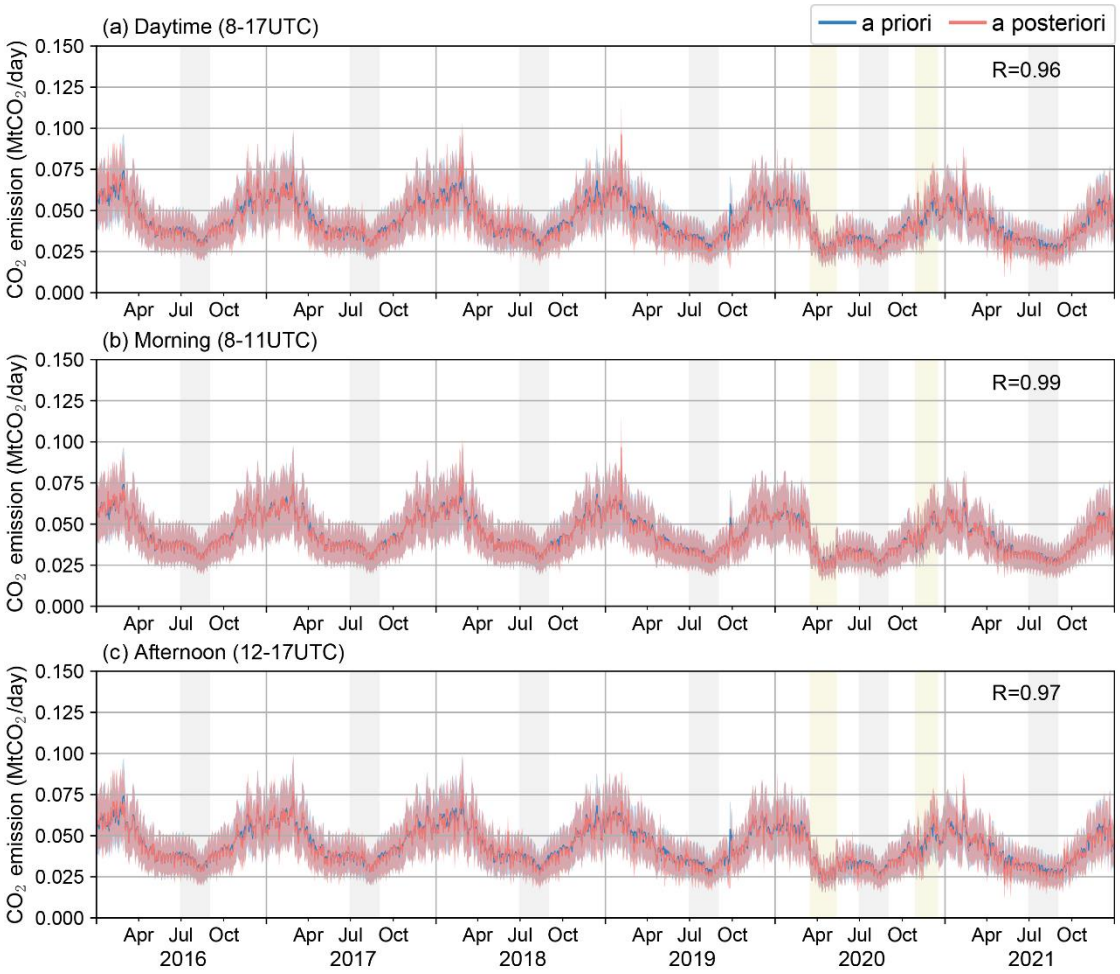

Figure S6. Daily estimates of fossil fuel CO_2 emissions over the rest of IdF region when assimilating (a) daytime (8-17UTC), (b) morning (8-11UTC) and (c) afternoon (12-17UTC) CO_2 concentration observations. The blue line and shading show the prior flux according to the Origins.earth inventory together with its assumed uncertainty. The pink and shading show the posterior estimates with their uncertainty ranges. The yellow shaded areas are the two COVID-19 lockdown periods in France. The grey shaded areas are the summer holidays of July and August.

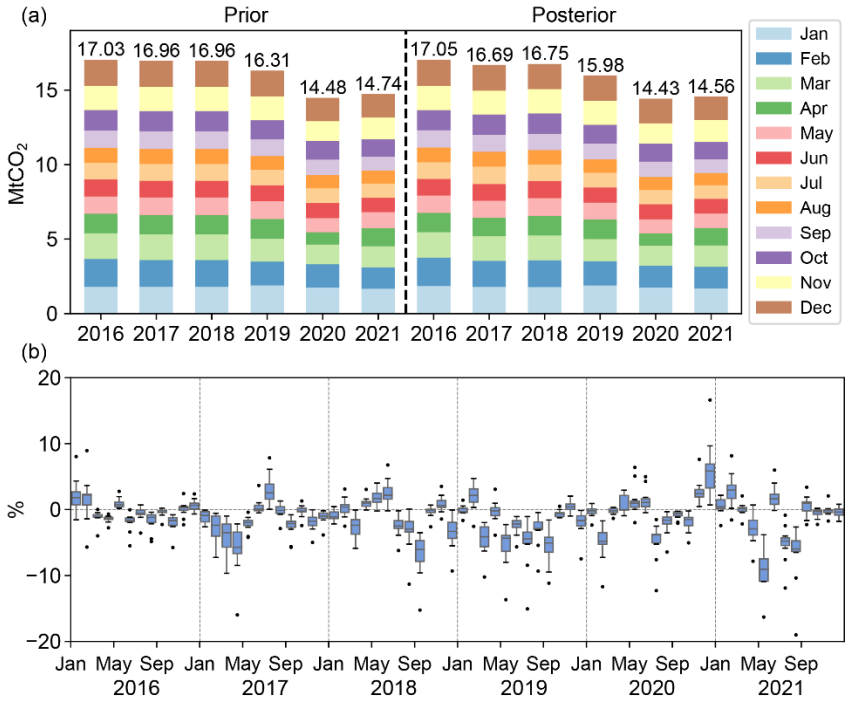

Figure S7. (a) Prior and posterior estimates of the monthly total fossil fuel CO_2 emission over the rest of IdF region. (b) the change of CO_2 emissions in percentage (posterior-prior)/prior. The boxplots are the posterior emissions from an ensemble of sensitivity tests of the inversion configuration.

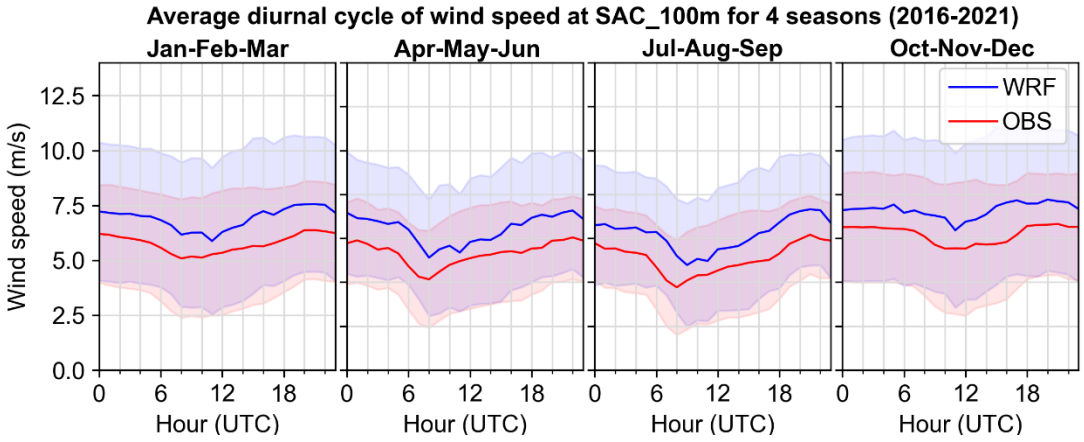

Figure S8. Average diurnal cycle and the standard deviation of the observed and modeled wind speeds at 100m above the ground level at SAC station for four seasons from 2016 to 2021.

Text ~~S4~~S3. Residential heating

Residential CO_2 emissions are typically determined by multiple energy consumption statistics accounting for fossil fuels and their corresponding emission factors. It usually includes petroleum, bottle gas, city gas, wood, and coal. Note that the electricity and urban network energy sources are included in the energy sector in the Origins.earth inventory and are therefore not accounted for here. The calculation of fossil fuel CO_2 emissions for the residential sector in the Origins.earth inventory follows two steps: (1) estimating the spatialized annual emissions from different energy consumption sources. (2) downscaling annual emission to the hourly time scale based on the domestic gas consumption data from the SmartGRT database (https://smart.grtgaz.com/en/consommation). This assumption of the evolution of emissions with time ignores the temporal variations of other energy sources for the residential sector (e.g., petroleum, wood, coal). We thus calculate the proportions of annual residential fossil fuel CO_2 emissions from different energy types (Figure S9). These shares indicate that the temporal variation of residential CO_2 emissions from petroleum and wood burning might be an important missing source in the Origins.earth inventory, especially in suburban areas.

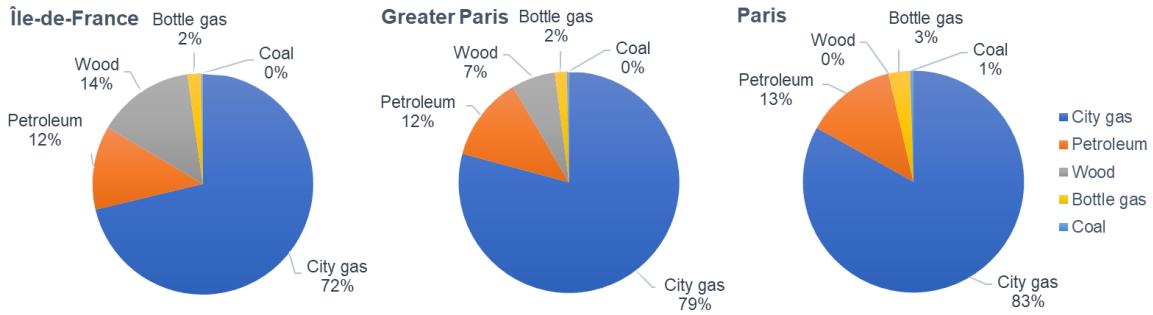

Figure S9. The proportions of annual residential fossil fuel CO_2 emissions from different energy types (in percentage) over Île-de-France, Greater Paris and Paris city respectively.

Text ~~S5~~S4. Biogenic flux

The VPRM modeled biogenic fluxes (net ecosystem exchange, NEE) are compared with the eddy flux measurements at two stations within the IdF region (Figure S10). The Fontainebleau forest site (48.4763°N; 2.7801°E) is located southeast of Paris center. Deciduous broadleaf trees (oak (Quercus petraea and Quercus robur), beech (Fagus sylvatica), and hornbeam (Carpinus betulus)) are the dominant species in the vicinity of the flux tower. The Grignon site (48.8442°N, 1.9519°E) is located at around 40 km west of Paris. The crop is a maize, winter-wheat, oilseed rape, winter-wheat rotation.

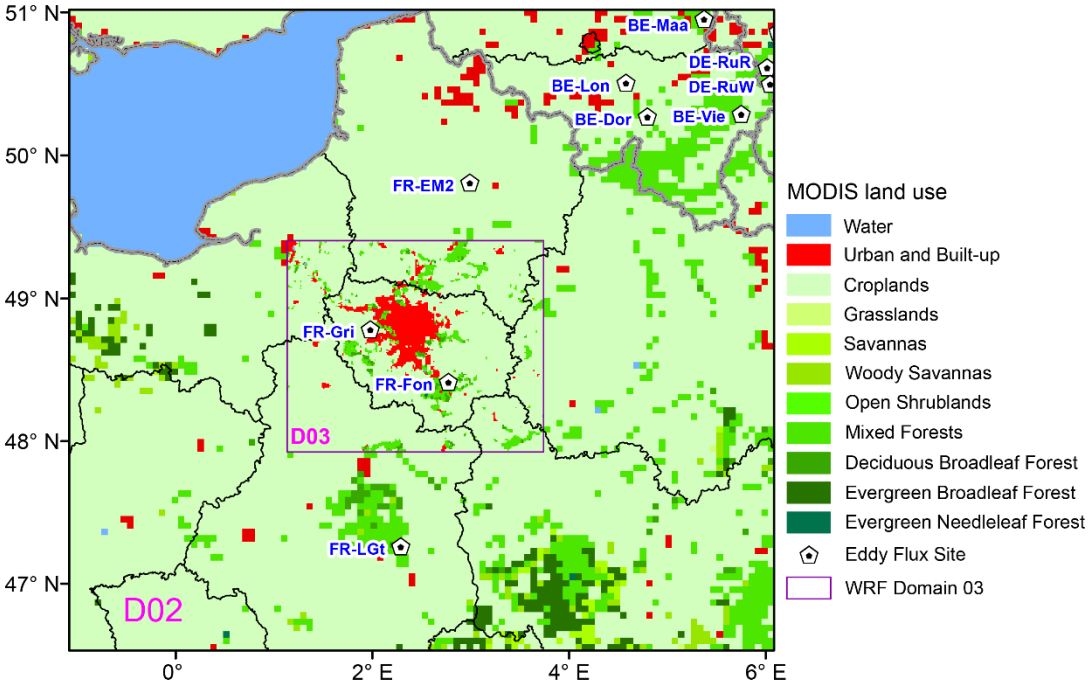

Figure S10. Locations of eddy flux stations within the inner two WRF domains (D02 and D03) together with the MODIS land use map.

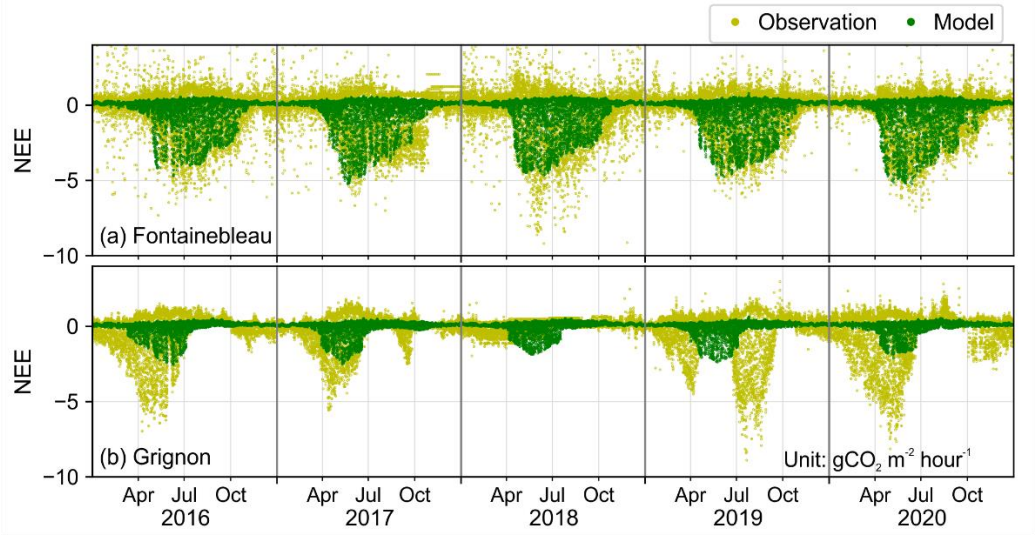

Figure S11. Comparison of the WRF-VPRM simulated hourly biogenic flux (net ecosystem exchange, NEE) with the measured eddy flux data at the (a) Fontainebleau forest station and (b) Grignon cropland station from 2016 to 2020.

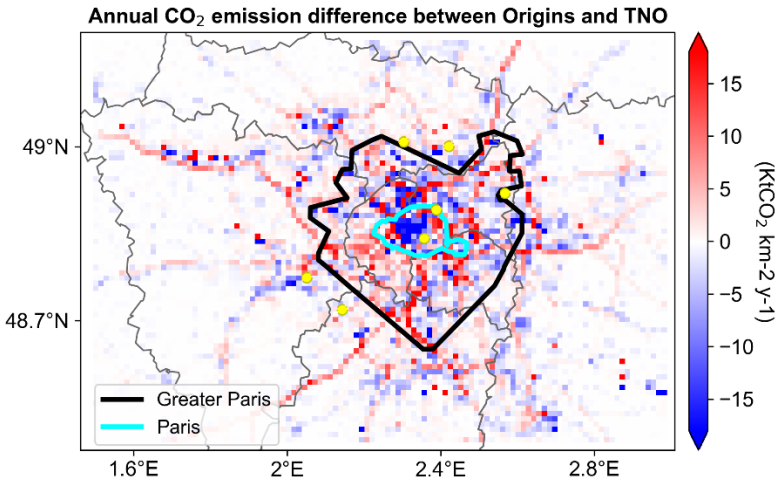

Figure S12. Differences in annual fossil fuel CO_2 emission between the Origins.earth and the TNO 1km inventory for the year 2018.

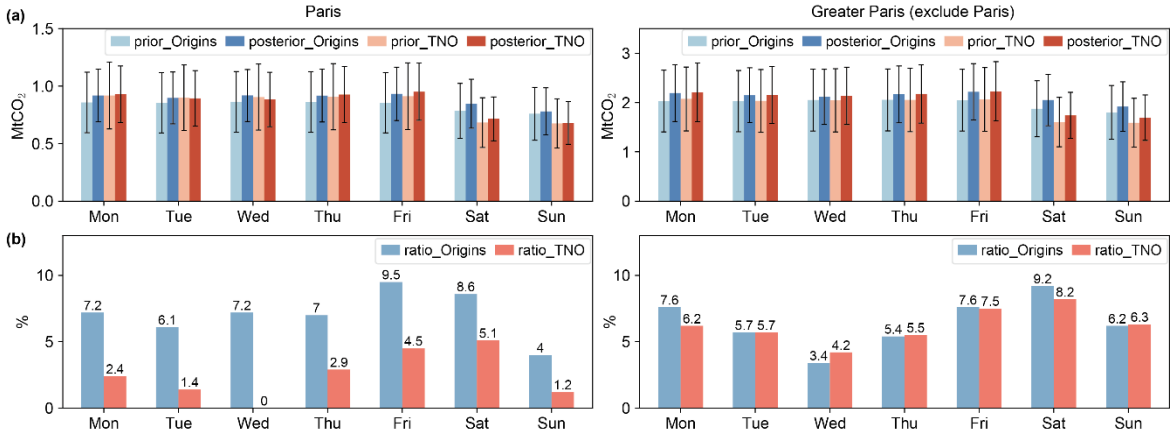

Figure S13. (a) Annual fossil fuel CO_2 emissions prior estimates by Origins.earth and TNO 1km inventory and the respective posterior estimates for the seven days of the week in 2018 over the city of Paris (left panel) and the rest of Greater Paris region (right panel) (cf. Figure S12) respectively. (b) the change of CO_2 emissions in percentage (posterior-prior)/prior.

SI References

Kotthaus, S., Bravo-Aranda, J. A., Collaud Coen, M., Guerrero-Rascado, J. L., Costa, M. J., Cimini, D., O'Connor, E. J., Hervo, M., Alados-Arboledas, L., Jiménez-Portaz, M., Mona, L., Ruffieux, D., Illingworth, A., and Haeffelin, M.: Atmospheric boundary layer height from ground-based remote sensing: a review of capabilities and limitations, Atmos. Meas. Tech., 16, 433–479, https://doi.org/10.5194/amt-16-433-2023, 2023.

Lian, J., Lauvaux, T., Utard, H., Broquet, G., Bréon, F.M., Ramonet, M., Laurent, O., Albarus, I., Cucchi, K., and Ciais, P.: Assessing the Effectiveness of an Urban CO_2 Monitoring Network over the Paris Region through the COVID-19 Lockdown Natural Experiment. Environmental Science & Technology, https://doi.org/10.1021/acs.est.1c04973, 2022.

Pôle de Coordination des Inventaires Territoriaux, Guide méthodologique pour l'élaboration des inventaires territoriaux des émissions atmosphériques, 2018, Ministère Chargé de l'Environnement. Available online: https://www.lcsqa.org/system/files/media/documents/MTES_Guide_methodo_elaboration_inventaires_PCIT_mars2019.pdf (accessed on 17 March 2022).